Cell Reports

Article

# A Three-Way Combinatorial CRISPR Screen for Analyzing Interactions among Druggable Targets

## Graphical Abstract

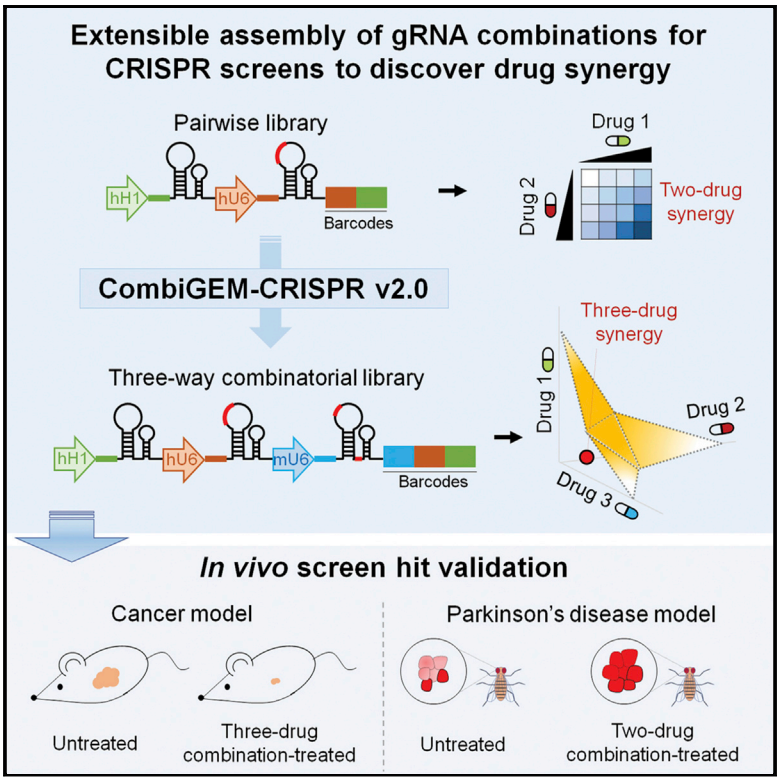


## Highlights

- Toolkits are engineered for extensible assembly of barcoded high-order gRNA arrays
- Simultaneous knockout of up to three genes for combinatorial CRISPR screening
- CRISPR screens identify infrequent synergistic interactions among druggable targets
- Gene interactions are translated to matching drugs for disease phenotype modulation


## Authors

Peng Zhou, Becky K.C. Chan, Yuk Kei Wan, ..., Koon Ho Wong, H.Y. Edwin Chan, Alan S.L. Wong

## Correspondence

aslw@hku.hk



## In Brief

Studying high-order druggable gene interactions that mimic the actions of targeted drug combinations is practically challenging. Zhou et al. describe an extensible CombiGEM-CRISPR system for screening high-order combinations, leading to identification of double- and triple-combination regimens that suppress ovarian cancer growth and Parkinson's disease-associated toxicity.


Zhou et al., 2020, Cell Reports *32*, 108020
August 11, 2020 
https://doi.org/10.1016/j.celrep.2020.108020

CellPress

Cell Reports

CellPress
OPEN ACCESS

Article

# A Three-Way Combinatorial CRISPR Screen for Analyzing Interactions among Druggable Targets

Peng Zhou,[1] Becky K.C. Chan,[1] Yuk Kei Wan,[1] Chaya T.L. Yuen,[1] Gigi C.G. Choi,[1] Xinran Li,[2] Cindy S.W. Tong,[1] Sophia S.W. Zhong,[1] Jieran Sun,[1] Yufan Bao,[3,4] Silvia Y.L. Mak,[3] Maggie Z.Y. Chow,[3] Jien Vei Khaw,[1] Suet Yi Leung,[5,6,7] Zongli Zheng,[3,4,8] Lydia W.T. Cheung,[2] Kaeling Tan,[9,10] Koon Ho Wong,[9,11] H.Y. Edwin Chan,[12,13] and Alan S.L. Wong[1,14,15,*]

[1]Laboratory of Combinatorial Genetics and Synthetic Biology, School of Biomedical Sciences, The University of Hong Kong, Pokfulam, Hong Kong SAR, China
[2]School of Biomedical Sciences, The University of Hong Kong, Pokfulam, Hong Kong SAR, China
[3]Ming Wai Lau Centre for Reparative Medicine, Karolinska Institutet, Hong Kong SAR, China
[4]Department of Biomedical Sciences, City University of Hong Kong, Hong Kong SAR, China
[5]Department of Pathology, The University of Hong Kong, Pokfulam, Hong Kong SAR, China
[6]Centre for PanorOmic Sciences, The University of Hong Kong, Pokfulam, Hong Kong SAR, China
[7]The Jockey Club Centre for Clinical Innovation and Discovery, LKS Faculty of Medicine, The University of Hong Kong, Pokfulam, Hong Kong SAR, China
[8]Biotechnology and Health Centre, City University of Hong Kong Shenzhen Research Institute, Shenzhen, China
[9]Faculty of Health Sciences, University of Macau, Macau SAR, China
[10]Genomics, Bioinformatics and Single Cell Analysis Core, Faculty of Health Sciences, University of Macau, Avenida da Universidade, Taipa, Macau SAR, China
[11]Institute of Translational Medicine, University of Macau, Avenida da Universidade, Taipa, Macau SAR, China
[12]Laboratory of *Drosophila* Research, School of Life Sciences, The Chinese University of Hong Kong, Hong Kong SAR, China
[13]Gerald Choa Neuroscience Centre, The Chinese University of Hong Kong, Hong Kong SAR, China
[14]Department of Electrical and Electronic Engineering, The University of Hong Kong, Pokfulam, Hong Kong SAR, China
[15]Lead Contact
*Correspondence: aslw@hku.hk
https://doi.org/10.1016/j.celrep.2020.108020

## SUMMARY

We present a CRISPR-based multi-gene knockout screening system and toolkits for extensible assembly of barcoded high-order combinatorial guide RNA libraries *en masse*. We apply this system for systematically identifying not only pairwise but also three-way synergistic therapeutic target combinations and successfully validate double- and triple-combination regimens for suppression of cancer cell growth and protection against Parkinson's disease-associated toxicity. This system overcomes the practical challenges of experimenting on a large number of high-order genetic and drug combinations and can be applied to uncover the rare synergistic interactions between druggable targets.

## INTRODUCTION

Despite the promise of combination therapies to enhance treatment efficacy for various diseases (Al-Lazikani et al., 2012), only a limited number of effective combinations, especially those comprising three or more drugs (Table S1), have been discovered so far. Drug combination effects are difficult to predict because of unanticipated synergies or antagonisms and are not simply the sum of the effects of each drug (Borisy et al., 2003). Microplate arrays are coupled to robotics systems to screen large panels of drug combinations. However, as the number of experiments grows exponentially with the number of drugs and the order of combinatorial complexity being studied, such an approach can become prohibitively expensive. RNA interference-based and clustered regularly interspaced short palindromic repeats (CRISPR)-based genetic perturbation systems have been applied to facilitate screening of effective drug target pairs (Doench, 2018; Wong et al., 2016b). The Combinatorial Genetics *En Masse* (CombiGEM)-CRISPR platform (Wong et al., 2015, 2016a) could, in theory, be used to generate high-order combinatorial guide RNA (gRNA) libraries, but the library assembly strategy was not optimized for screening of three or more targets simultaneously. The extensibility of other existing methods for screening high-order genetic combinations is also limited by the relatively low and variable cleavage efficiency for polycistronic systems to express multiple RNAs (Han et al., 2017; Xu et al., 2017), and/or characterization of high-order combinations requires large-scale oligo synthesis and high sequencing costs (elaborated in Design of CombiGEM-CRISPR v.2.0). Mathematical models have been developed for predicting three-way and higher-order drug interactions (Cokol et al., 2017; Wood et al., 2012; Zimmer et al., 2016), but high-throughput methods are

**Table 1. Evaluation of the Extensibility of Existing Methods and Possible Toolkits for Assembling Three-Way gRNA Combinations for Screening**

| Possible Strategy for Assembling a Three-way CRISPR Screening Library | Oligos Needed for a Three-Way Library with "m" gRNAs/crRNAs | Large-Scale Bacterial Transformation Required for Library Cloning | Expression Levels of Multiple gRNAs/crRNAs | Expression of CRISPR Enzyme(s) in the Screening Cell Line | Next-Generation Sequencing Cost |
|---|---|---|---|---|---|
| Synthesis of (barcoded [BC]) gRNA spacer array (with <170 bp), followed by sequential insertion of (1) scaffold/promoter sequences or (2) scaffold/processing sites | more ($m \times m \times m = m^3$ oligos, which include all possible three-way combinations of gRNA spacers) | multiple steps (all intermediate cloning steps until the final assembly step) | high (for [1])/potentially lower (for [2]) (a relatively low and variable cleavage efficiency for the polycistronic Csy4 system to express multiple gRNA was reported; Han et al., 2017) | SpCas9 (and Csy4 when Csy4 processing sites are used) | lower (with barcode)/higher (without barcode) (for the barcoded array, <50 bp [single-read]; for the non-barcoded array, ~400 – 800 bp [long read], or for (2), ~250 bp + ~20 bp [paired-end read]) |
| Gibson/Golden Gate assembly of multiple individual gRNA expression cassettes | less (m pairs of oligos for cloning into individual expression cassettes) | one step (only at the final assembly step) | high | SpCas9 (and saCas9 when the orthologous Cas9 system is used; Najm et al., 2018) | higher (for [1], ~800 bp (long read); for [ii], ~200 bp + ~20 bp [paired-end read], but inverted repeat sequence being introduced may cause its instability in the genome) |
| CombiGEM-based assembly of barcoded gRNA expression cassettes | less (m pairs of oligos for cloning into individual expression cassettes) | one step (only at the final assembly step) | high | SpCas9 | lower, fewer than 50 bp (single read) |
| Synthesis of the crRNA array (each oligo with >200 bp) | more and longer ($m \times m \times m = m^3$ oligos, which include all possible three-way combinations of crRNAs together with scaffold and direct repeat (DR) sequences) | one step (only at the final assembly step) | potentially lower | Cpf1 | lower, ~250 bp (single read) or ~150 bp + ~80 bp (paired-end read) |

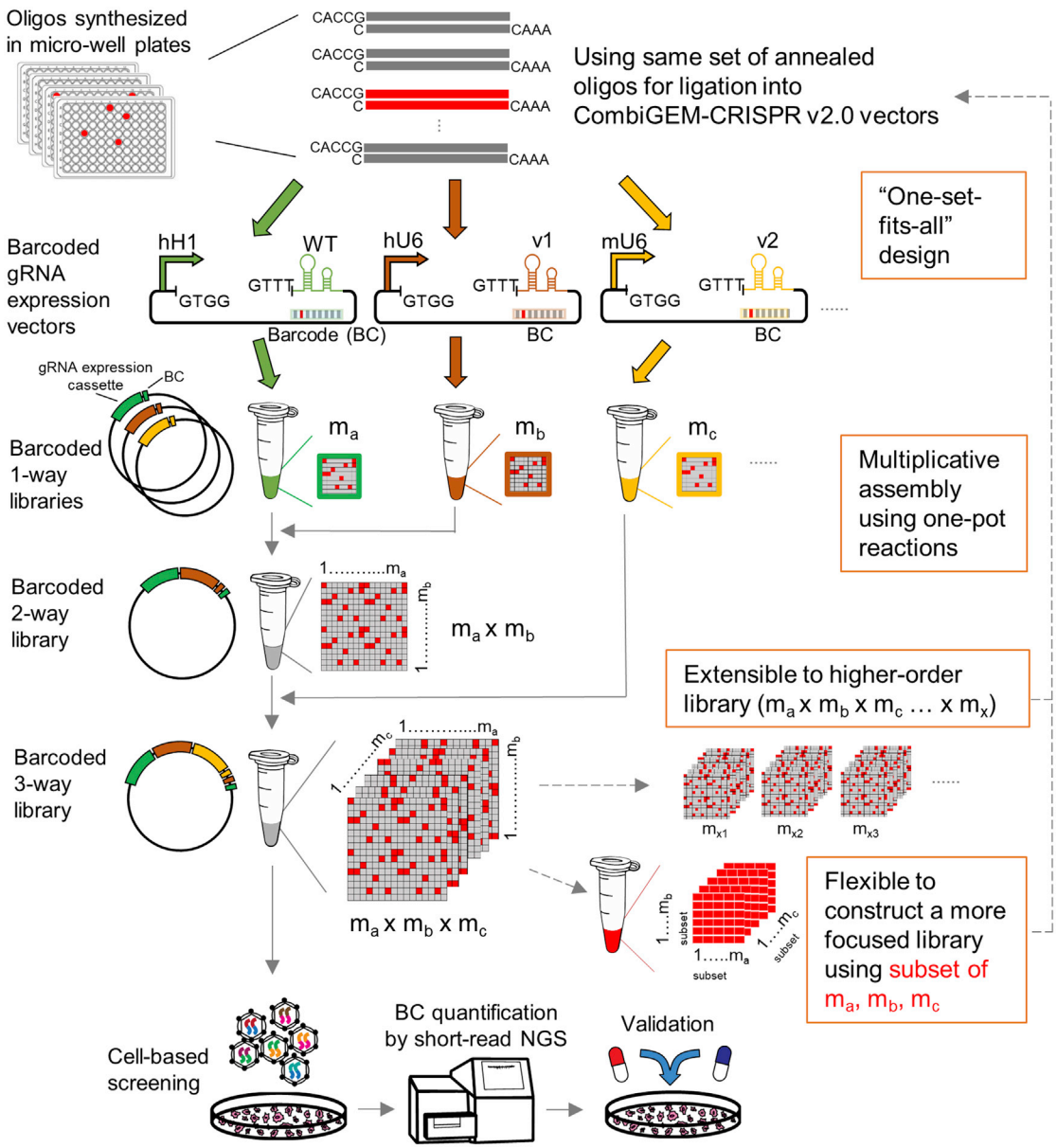


**Figure 1. Overview of CombiGEM-CRISPR v.2.0**

The workflow starts with synthesis of barcoded gRNA oligo pairs, which are annealed and cloned into gRNA expression vectors in a pooled format. Only one set of oligos is needed for building the libraries of higher-order gRNA combinations for multiplexed CRISPR screens because the 3′ ends of promoters are sequence-adapted to the sticky ends of the annealed oligos. A barcoded combinatorial gRNA library is assembled multiplicatively using one-pot reactions and delivered into human cells by lentiviruses. Barcoded representations within cell pools are quantified using next-generation sequencing. Then, validation is done by using matching drugs. Pre-assembled libraries can also be flexibly extended to higher-order ones, or a more focused library can be constructed using a subset of the same oligos for a secondary screen. See also Figure S1.

needed to experimentally validate sets of potential combinations. Breaking through the bottlenecks, here we establish and validate the second generation (v.2.0) of the CombiGEM-CRISPR platform for rapid screening of disease-alleviating gene knockouts to study high-order genetic interactions, identify potential therapeutic target combinations, and deploy their matching drug regimens for further testing.

## RESULTS

### Design of CombiGEM-CRISPR v.2.0

CombiGEM-CRISPR v.2.0 toolkits include add-on designs on library vectors that enable only a single reusable set of oligos to be synthesized for performing high-order combinatorial CRISPR screens. We and others have shown that CRISPR screens can

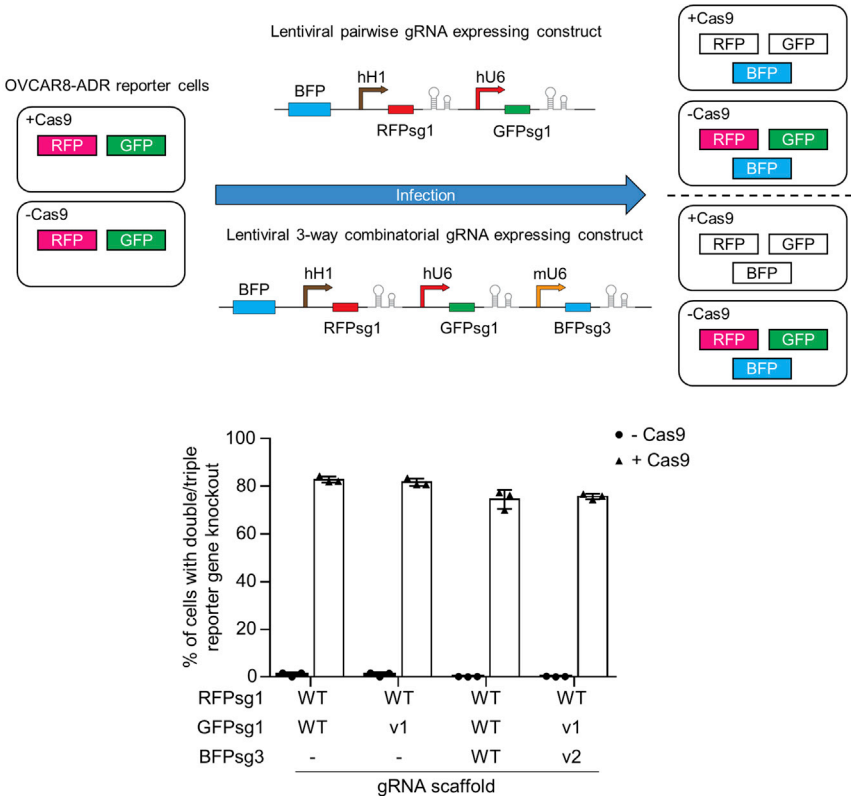


**Figure 2. Functional Disruption of Multiple Genes Using a CRISPR-Cas9-Based Multigene Knockout System**

Lentiviral delivery of combinatorial gRNA expression constructs efficiently disrupts multiple target genes. Flow cytometry was used to measure the percentage of cell populations positive for GFP, RFP, and BFP on days 11–14 post-infection in OVCAR8-ADR and OVCAR8-ADR-Cas9 cells. Data are mean ± SD; n = 3 biological replicates. See also Figure S2.

be carried out by targeting two genes simultaneously using dual gRNA expression cassettes (Chow et al., 2019; Du et al., 2017; Han et al., 2017; Najm et al., 2018; Shen et al., 2017; Wong et al., 2016a). Here we evaluated the extensibility of existing methods and other possible toolkits for assembling a three-way combinatorial gRNA library for screening (Table 1). Considering using an oligo synthesis-based approach to build a library with $m_a \times m_b \times m_c$ combinations, the same number of gRNA protospacers-containing oligos (i.e., $m_a \times m_b \times m_c$) has to first be designed and synthesized to include all combinations and followed by sequential insertions of the promoter and scaffold sequences. The drawbacks are that (1) all intermediate cloning steps require large-scale bacterial transformations for maintaining high library coverage, which is technically more demanding than the CombiGEM-CRISPR v.2.0 method, which only requires a large-scale transformation at the final assembly step, and (2) the rigid cloning framework does not permit post-assembly insertion of additional gRNAs for building higher-order libraries. The inflexible workflow also limits reusability of oligos for building a more compact library for secondary screens. For example, if a pairwise gRNA library was constructed for identifying the core effectors to be included in a three-way gRNA library, then building of the higher-order library requires additional sets of oligos to be synthesized for complete re-assembly of libraries. Alternative library assembly strategies are through Gibson-based (Gibson et al., 2009) or Golden Gate-based (Engler et al., 2008) methods, which require designing overlapping regions or complementary overhangs of adjacent gRNA expression units for fusing multiple parts together. However, these methods also do not allow additional parts to be introduced to pre-existing barcoded libraries. Our CombiGEM-CRISPR v.2.0 strategy provides a truly scalable solution that enables multiplicative assembly of additional barcoded gRNA expression units for extending from n to n+1 combinatorial CRISPR libraries (Figure 1). Libraries can be also tailored and re-assembled from selected gRNAs by choosing from the suite of gRNAs stored in vectors for another screen or a secondary screen for higher resolution. In addition, creation of barcodes that are unique for each assembled combination allows their rapid characterization to be performed via short sequencing reads, which reduces sequencing cost and potential errors generated via long reads. We therefore decided to take this approach to build three-way combinatorial gRNA libraries for screening applications.

Because previous CombiGEM toolkits were not directly adaptable for assembling three-way and even higher-order combinatorial gRNA libraries, here we further created a "one set fits all" design so that building an n-way combinatorial CRISPR screening library of m gRNAs using multiple gRNA expression cassettes always requires only m (instead of n × m) pairs of oligos to be synthesized. To ensure expression of three gRNAs in single cells, we assembled the multiple gRNA expression cassettes in a single vector. Multiple promoters (including human U6, mouse U6, and human H1) (Adamson et al., 2016; Ma et al., 2014; Vidigal and Ventura, 2015) and modified gRNA scaffolds (Adamson et al., 2016; Briner et al., 2014; Dang et al., 2015; Grevet et al., 2018) were used in the expression cassettes (Figure S1A), which minimizes possible lentiviral vector recombination because of long homologous sequences. However, use of multiple promoters requires multiple sets of oligos and/or additional PCR and restriction enzyme digestion reactions for building the different expression cassettes for library assembly. To allow researchers synthesizing and annealing only a single set of oligos as parts to build all possible higher-order combinations of gRNAs for multiplexed CRISPR screens, we performed sequence adaptation by modifying the 3′ end sequence of promoters to those that are complementary to the sticky ends of the annealed oligos, and these promoters expressed gRNAs

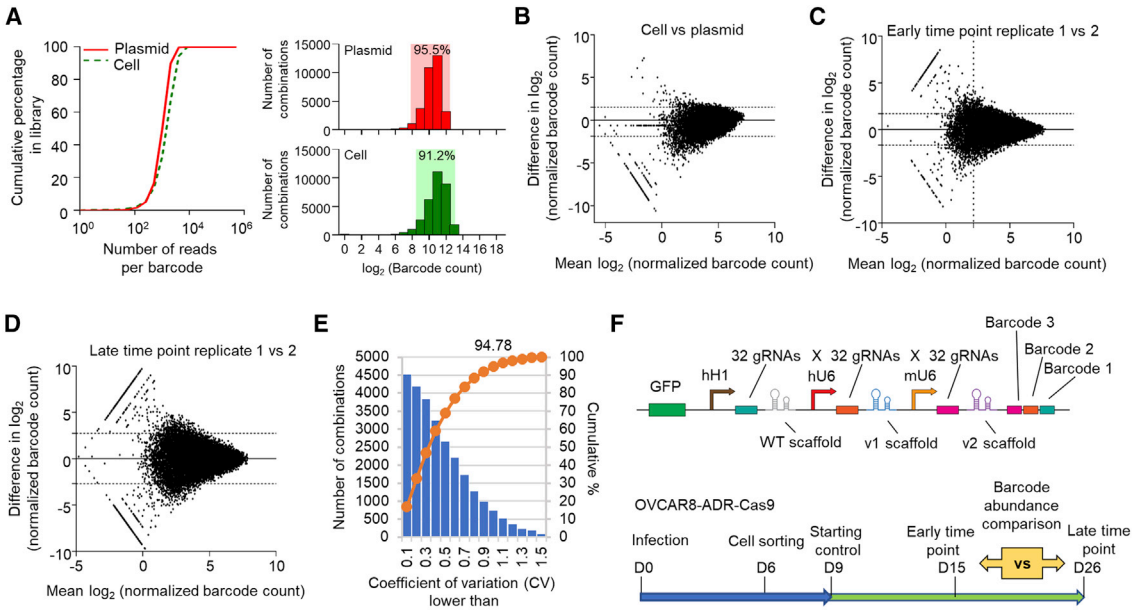


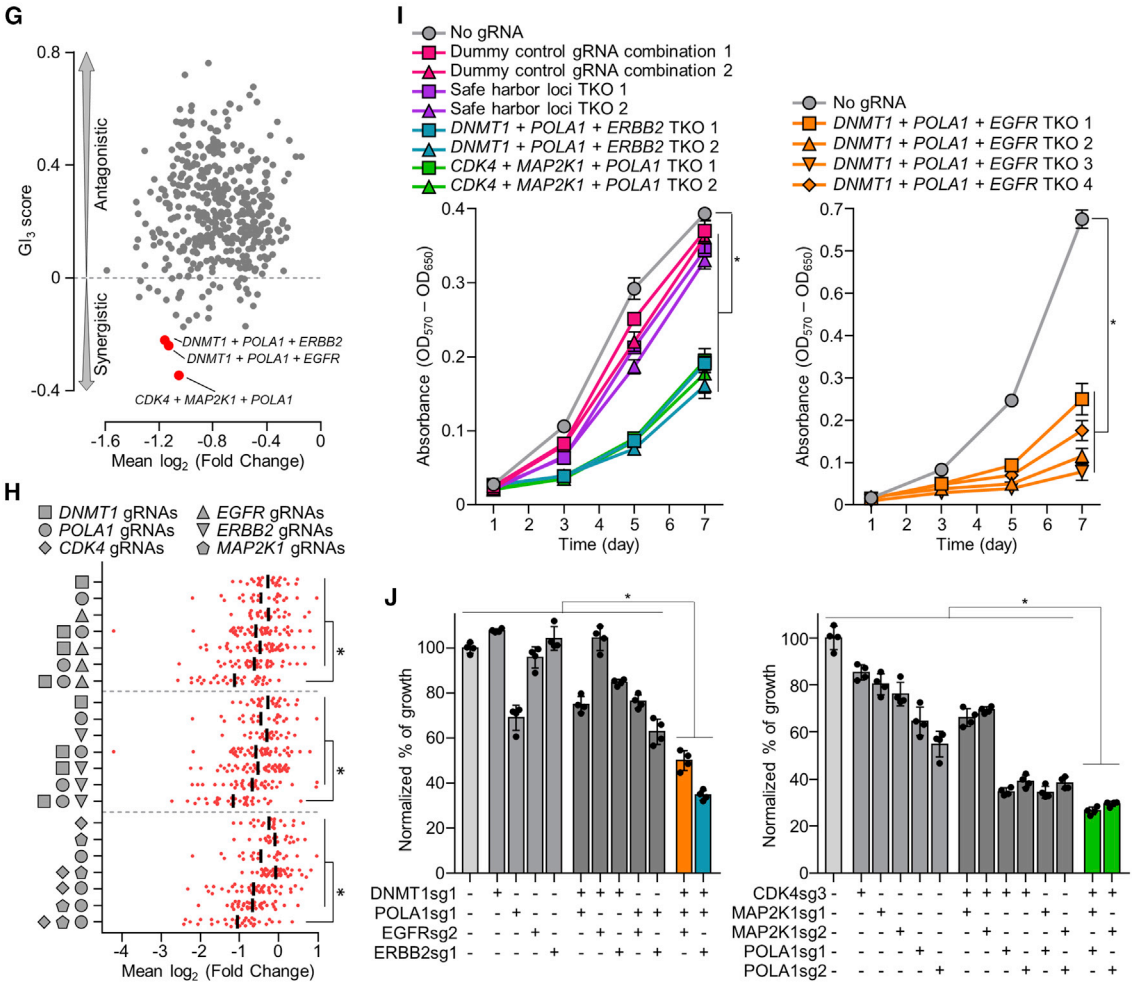


*(legend on next page)*

and generated efficient gene knockouts (Figure S1B). These standardized vector parts are useful for flexible assembly of high-order combinatorial gRNA libraries and extensible combinatorial CRISPR screens.

### Establishment of a CRISPR-Cas9-Based Multi-gene Knockout System

We constructed a lentiviral combinatorial gRNA expression vector containing multiple gRNA expression cassettes to efficiently and simultaneously knock out three target genes (Figure 2) and evaluated its functionality in human cells (OVCAR8-ADR) using gRNAs targeting the exonic regions of green fluorescent protein (GFP), red fluorescent protein (RFP), and blue fluorescent protein (BFP) reporter genes. Lentiviruses carrying a BFP reporter and the combinatorial gRNA units were generated to infect OVCAR8-ADR and OVCAR8-ADR-Cas9 cells stably expressing RFP and GFP reporters. Flow cytometry analysis was performed to confirm effective generation of double and triple knockout of the reporter proteins (>81% and >74%, respectively) (Figures 2 and S2A). Similar knockout efficiencies were observed when wild-type (WT) or modified gRNA scaffolds were used. Swapping the promoters driving gRNA expression also resulted in similar knockout efficiencies (Figure S2B), suggesting that there was no promoter usage bias and that similar amounts of gRNAs were generated to evenly knock out individual genes. Our results indicate that the lentiviral vector can be used to deliver gRNAs to generate multi-gene knockouts, and this vector design was used for the combinatorial CRISPR-Cas9 screens in this study.

### A Three-Way Combinatorial CRISPR-Cas9 Screen for Synergistic Anti-cancer Genetic Combinations

Combinatorial drug therapy targeting multiple pathways can limit development of drug-resistant phenotypes in cancer cells because it is harder for the cells to activate multiple compensatory survival mechanisms (Bozic et al., 2013). We performed high-throughput studies to search for effective therapeutic combinations against high-grade serous ovarian cancer (HGSOC), the most prevalent subtype that contributes to two-thirds of all ovarian cancer deaths (Bowtell, 2010). With the CRISPR-based multi-gene knockout system described above, we applied CombiGEM-CRISPR v.2.0 to assemble a high-coverage (99.8%), three-way combinatorial gRNA library (with 32 × 32 × 32 gRNAs = 32,768 total combinations) (Figures 3A–3E). This library included 15 druggable protein-encoding genes (with 2 gRNAs per gene) that are commonly targeted in anti-cancer therapies and whose expressions have been reported in OVCAR8-ADR, an established cell model of HGSOC (Baratta et al., 2015), and also other ovarian cancer cells based on the NCI-60 proteome database (Gholami et al., 2013) to demonstrate the feasibility of our approach (Tables S2 and S3). To generate combinatorial gene knockouts at a high rate, we selected gRNAs with predicted high on-target (and low off-target) activities based on the Azimuth 2.0 model (Doench et al., 2016). We compared the on-target efficacy score and the insertion or deletion (indel) generation efficiency of gRNAs and observed that the on-target efficacy score largely predicts the efficiency of gRNAs in OVCAR8-ADR cells (Figure S3A). We chose gRNAs that have on-target scores of more than 0.64 based on the Azimuth 2.0 model, and most of them also have high frameshift generation rates analyzed under the newly developed inDelphi and FORECasT (Favoured Outcomes of Repair Events at Cas9 Targets) models (Figure S3B; Allen et al., 2018; Shen et al., 2018). GUIDE-seq (Genome-wide, Unbiased Identification of DSBs Enabled by Sequencing) was performed to evaluate the genome-wide cleavage activities of Cas9 and showed that the combinatorial gene knockouts generated by the three selected gRNAs were highly specific and that the three-way gene knockout did not increase off-target edits compared with the

**Figure 3. A CRISPR-Based Triple-Gene Knockout Screen Identifies Synergistic Three-Way Combinations that Inhibit Ovarian Cancer Cell Growth**

(A) Distributions of barcode reads in the plasmid and infected OVCAR8-ADR-Cas9 cell pools. A high-coverage three-way combinatorial gRNA library (99.8% of all expected gRNA combinations; 32,705 of 32,768) was obtained in the plasmid and cell pools. Most barcoded gRNA combinations were detected within a 5-fold range from the mean barcode reads per combination (highlighted by the shaded areas).

(B) High correlation between barcode representations (normalized barcode counts) within the plasmid pool and infected cell pool indicates efficient lentiviral delivery of the three-way combinatorial gRNA library into cells. The horizontal dotted lines in the Bland-Altman plots indicate the 95% limits of agreement.

(C and D) High reproducibility for barcode representations between two biological replicates in cells cultured for 15 days (C) and 26 days (D) post-infection with the three-way combinatorial gRNA library. The horizontal dotted lines in the Bland-Altman plots indicate the 95% limits of agreement. The vertical dashed line indicates the threshold of 100 raw barcode counts.

(E) The coefficient of variation (CV; defined as SD/mean of the fold changes of normalized barcode counts for 26-day versus 15-day cultured cells) was determined for the two biological replicates. Over 94.8% of pairwise gRNA combinations had a CV of less than 1 in the screen.

(F) OVCAR8-ADR-Cas9 cells infected with the barcoded three-way combinatorial gRNA library were cultured for 15 and 26 days. Barcode representations within the cell pools were quantified using Illumina HiSeq. The barcoded library vector uses an hH1-gRNA-WT scaffold, hU6-gRNA-v1 scaffold, and mU6-gRNA-v2 scaffold in the first, second, and third expression cassettes, respectively.

(G) A plot of screen data showing the abundance changes of each barcoded gRNA combination on day 26 versus day 15 post-infection (in mean $\log_2$ [fold change], x axis) and their genetic interaction ($GI_3$) score (y axis). Hit combinations (*DNMT1* + *POLA1* + *EGFR*, *DNMT1* + *POLA1* + *ERBB2*, and *CDK4* + *MAP2K1* +*POLA1*) are highlighted in red. Data were collected from two biological replicates.

(H) Comparisons of the mean $\log_2$ (fold change) of three-way gRNA hit combinations with their constituent single and pairwise gRNA combinations (see STAR Methods for details). Statistical significance was analyzed by one-way ANOVA with Dunnett's post hoc test. *$p < 0.05$.

(I and J) OVCAR8-ADR-Cas9 cells were infected with triple-gRNA combinations that target the indicated genes (I) and the respective single and/or double-gRNA combinations (J). The three safe harbor loci being targeted were *PPP1R12C*, *THUMPD3-AS1*, and *CCR5*. The gRNAs used in each combination are listed in Table S3. Cell viability was determined by MTT assay. Data are mean ± SD from biological replicates (n = 4). Statistical significance was analyzed by one-way ANOVA with Dunnett's post hoc test, comparing the no-gRNA control with triple-gRNA combinations (I) or triple-gRNA combinations with the respective single and double gRNAs (J). *$p < 0.05$.

See also Figure S3.

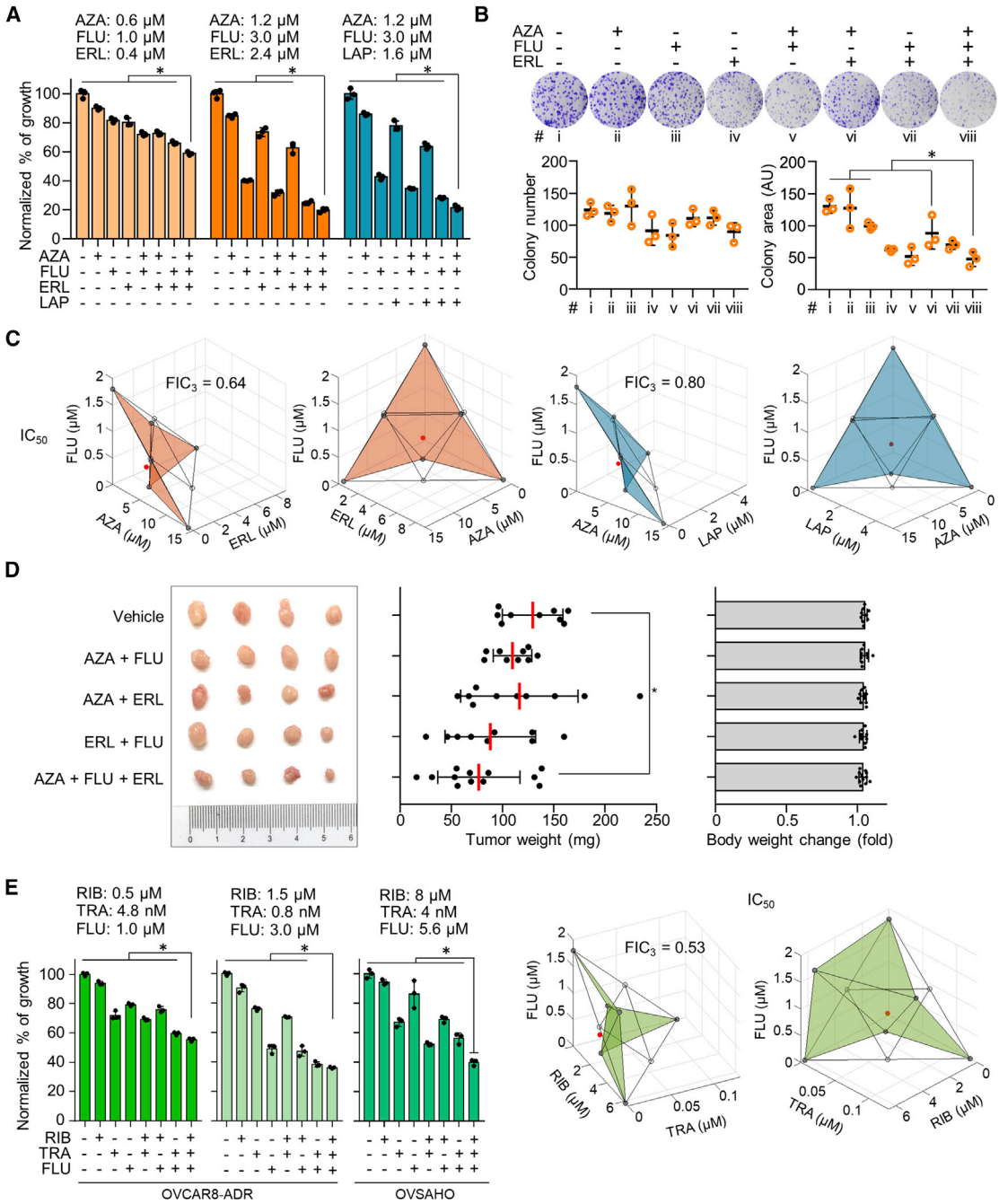


**Figure 4. Suppression of Ovarian Cancer Cell Growth by Three-Drug Regimens Matched for the Genetic Screen Hits**

(A) Viability, determined by MTT assay, of OVCAR8-ADR cells treated with AZA, FLU, and/or ERL. Data shown are mean ± SD from biological replicates (n = 3). Statistical significance was analyzed by one-way ANOVA with Dunnett's post hoc test. *p < 0.05.

(B) Colony formation assay of AZA-, FLU-, and/or ERL-treated OVCAR8-ADR cells. The colony numbers and areas were quantified. Data shown are mean ± SD from biological replicates (n = 3). Statistical significance was analyzed by one-way ANOVA with Dunnett's post hoc test. *p < 0.05.

(C) Surface plots depict the drug synergy of AZA + FLU + ERL (orange) and AZA + FLU + LAP (cyan). Circles on the transparent triangular plane indicate the expected $IC_{50}$ for each two-drug combination, and the expected $IC_{50}$ for triple-drug treatment is located at the center of this triangle. Gray dots are the observed $IC_{50}$ values for single- and double-drug treatments. Red dots are the observed $IC_{50}$ values for the triple-drug treatments. Concave or convex colored planes indicate synergistic or antagonistic drug interactions, respectively. $FIC_3$ is the fractional inhibitory concentration. Views from two angles are displayed (left and right panels).

(D) Representative images of resected tumors formed by subcutaneous implantation of OVCAR8-ADR cells into BALB/cAnN-nu mice followed by drug treatment. The weights of the tumors and body weights of the mice were measured. The data presented are compared among groups using one-way ANOVA with Tukey's post hoc test. *p < 0.05.

*(legend continued on next page)*

dual- and single-gene knockouts (Figure S3C). Two non-targeting control gRNAs from the Genome-Scale CRISPR Knockoout (GeCKO) v2 library (Shalem et al., 2014) that do not have on-target loci in the human genome were also included in the library as references.

We then conducted a pooled screen to isolate three-way gRNA combinations that modulate OVCAR8-ADR growth (Figure 3F). Barcode abundances of the day 15 and day 26 groups were compared to yield $\log_2$ values as a measure of cell growth. Based on the genetic screen data, 3 (of 455) three-way gene combinations had a mean $\log_2$ ratios of less than −1 (based on data obtained from two biological replicates with at least 50% fewer barcode counts in day 26- versus day 15-cultured cells) and a genetic interaction ($GI_3$) score of less than −0.2 (Figure 3G; Table S4). These three-way combinations (targeting *DNMT1* + *POLA1* + *EGFR* or *ERBB2* as well as *CDK4* + *MAP2K1*+ *POLA1*) also showed significantly different growth-modulatory effects from their respective single and pairwise combinations (Figure 3H; Table S4). Because they showed strong growth-inhibitory effects and strong synergistic genetic interactions, the three combinations were selected for further characterization. Their growth inhibition effects (reduced by 51.4% to 88.4% for the six tested gRNA combinations for *DNMT1* + *POLA1* + *EGFR* or *ERBB2* and reduced by 50.5% and 54.9% for the two tested gRNA combinations for *CDK4* + *MAP2K1*+ *POLA1*) were further confirmed by individual non-pooled assays and were not false positives caused by excessive double-strand DNB breaks generated by CRISPR-Cas9 (Aguirre et al., 2016; Munoz et al., 2016) because simultaneous targeting of three safe harbor loci did not result in strong growth arrest (Figures 3I, 3J, and S3D). The DNA copy numbers of *DNMT1*, *POLA1*, *EGFR*, *ERBB2*, *CDK4*, and *MAP2K1* loci were also largely not amplified in OVCAR8-ADR's genome based on analysis using CellMiner (Reinhold et al., 2012). CRISPR-Cas9-induced double-strand DNA breaks have been reported to result in indel generation as well as large deletion and sequence rearrangements (Kosicki et al., 2018; Shin et al., 2017). We determined the majority of the modifications to be indels of less than 200 bp located around the target sites of the gRNAs, and some edited alleles contained larger deletions and rearrangements within the targeted gene sequence (Figures S3D and S3E). These results suggest that growth inhibition resulting from gRNA expression was likely due to the targeted gene disruption.

## Hit Validation of an Anti-cancer Genetic Screen with Matching Three-Drug Combinations

Azacitidine (AZA), fludarabine (FLU), and erlotinib (ERL) were used to target DNMT1, POLA1, and EGFR, respectively. Lapatinib (LAP) was used to inhibit ERBB2, and it also acts on EGFR, which belongs to the same Erb protein family. The three-drug treatment of AZA, FLU, and ERL/LAP showed significantly stronger growth-inhibitory effects than the single- and double-drug treatments (Figures 4A and S4B) and resulted in a different set of perturbed genes, including those involved in cell cycle regulation, when comparing cells treated with the three-drug regimen with all of the respective two-drug combinations (Figure S4A). Furthermore, fewer G2 phase-arrested cells stained positive for pH3 after AZA + FLU + ERL treatment, suggesting reduced mitotic entry (Figure S4B). Synergy among the three drugs suppressing ovarian cancer cell growth was confirmed using the DiaMOND (diagonal measurement of *n*-way drug interactions) scoring method (Figure 4C; Cokol et al., 2017). The fractional inhibitory concentration (FIC) scores for AZA + FLU + ERL and AZA + FLU + LAP were 0.64 and 0.8, respectively, in OVCAR8-ADR cells. By comparing the drug dose required for achieving a half-maximal inhibiting concentration ($IC_{50}$) upon single-, double- and triple-drug treatments, we found that the triple-drug formulation of AZA + FLU + ERL demanded ~4.5-fold less of each component (and ~3.7-fold less for AZA + FLU + LAP). Similar results were observed when measuring other inhibitory concentrations ($IC_{30}$, $IC_{40}$, and $IC_{60}$; Figure S5A). In addition, the synergy among the three drugs (AZA + FLU + ERL or LAP) was detected in OVSAHO cells (Figure S5B). A significant decrease in tumor weight was detected in mice treated with the AZA + FLU + ERL formulation, whereas no behavior abnormalities and changes in body weight were observed, indicating minimal side effects induced by the drug interactions (Figure 4D). We also confirmed the synergy among the three matching drugs (ribociclib [RIB] + trametinib [TRA] + FLU) for our third screen hit (i.e., CDK4 + MAP2K1 + POLA1) in suppressing growth of OVCAR8-ADR and OVSAHO cells (Figure 4E). These results indicate that our platform enables high-throughput screening and identification of synergistic three-way therapeutic combinations.

## A CRISPR-Cas9 Screen for Drug Pairs against Ovarian Cancer

CombiGEM-CRISPR v.2.0 can also be applied for building libraries with more druggable targets and analyze their pairwise interactions. Via one-pot reactions (Figure S1B), we built a paired gRNA library targeting 52 druggable genes (3 gRNAs per gene; Tables S2 and S3) whose expressions have been shown in OVCAR8-ADR and also other ovarian cancer cells based on the NCI-60 proteome database (Gholami et al., 2013). We selected gRNAs with on-target scores of higher than 0.63 (with a predicted efficiency of more than ~80%), except for one with a score of 0.60. Three control gRNAs from the GeCKOv2 library (Shalem et al., 2014) that do not have on-target loci in the human genome were included as references. The pairwise gRNA library pool (with 159 × 159 gRNAs = 25,281 total combinations) was then delivered into OVCAR8-ADR cells via lentiviruses. Using our established experimental pipeline (Wong et al., 2015, 2016a), we performed Illumina HiSeq to confirm the high coverage (>99.0%) of the pairwise library and high correlation of barcode representation between the plasmid and infected cell pools (Figures 5A–5E). Using similar time windows as used

(E) Viability, determined by MTT assay (left panels), of OVCAR8-ADR/OVSAHO cells treated with RIB, TRA, and/or FLU. Data shown are mean ± SD from biological replicates (n = 3). Statistical significance was analyzed by one-way ANOVA with Dunnett's post hoc test. *$p < 0.05$. Surface plots (right panels) depict the drug synergy of RIB + TRA + FLU in OVCAR8-ADR, as presented in (C).
See also Figures S4 and S5.

CellPress
OPEN ACCESS

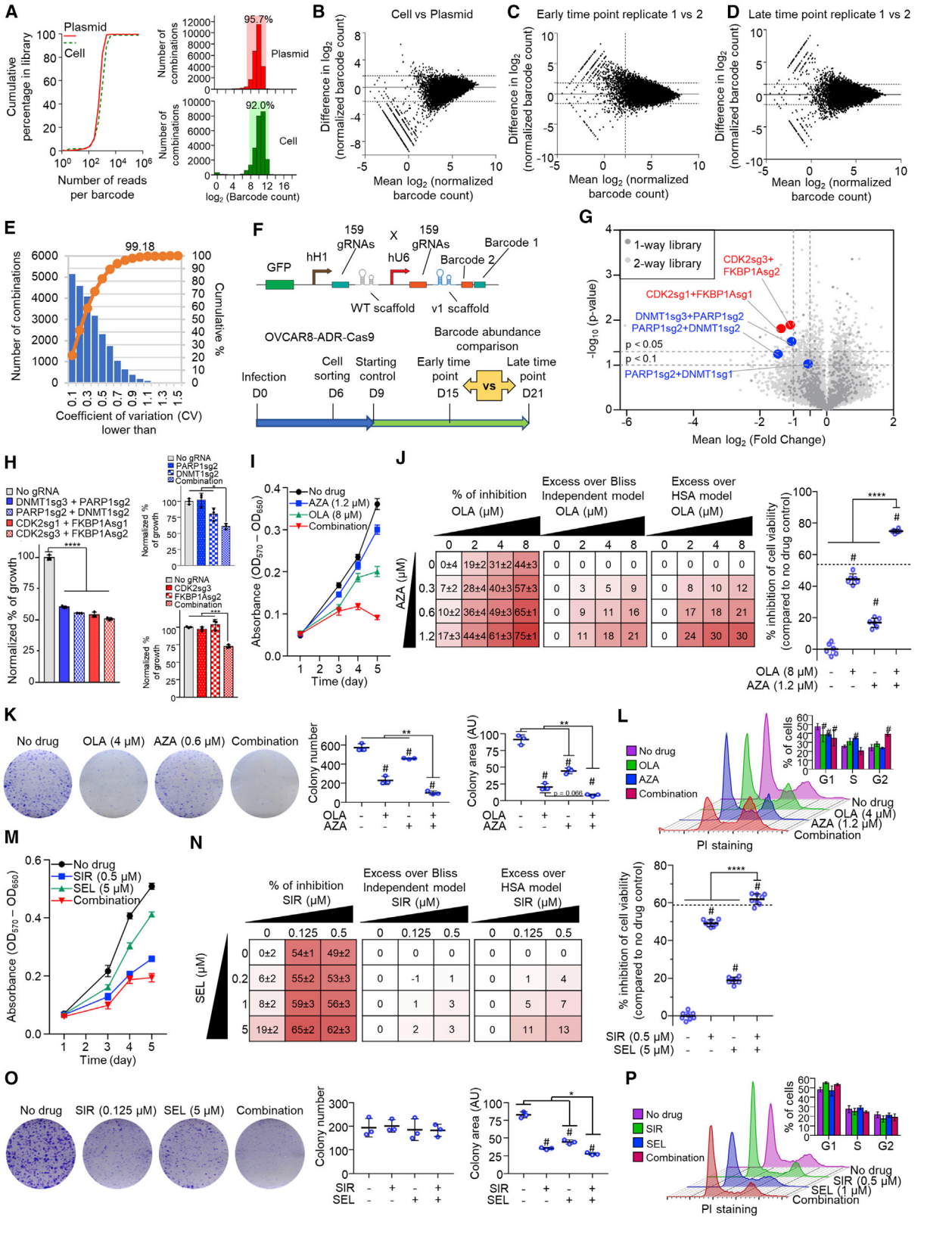


*(legend on next page)*

in our previous study, barcode abundances between the day 15 and day 21 groups were compared to yield log2 values as a measure of cell growth (Figure 5F). Based on selection criteria that required a mean log2 ratio of less than −1 (based on data obtained from two biological replicates with at least 50% fewer barcode counts in day 21- versus day 15-cultured cells) and multiple gRNAs targeting the same gene pair being detected with at least $p < 0.1$, two combinations (PARP1 + DNMT1 and CDK2 + FKBP1A, highlighted in blue and red, respectively, in Figure 5G) were defined as top screen hits. The growth inhibition brought by these two dual-gene knockouts was validated using individual non-pooled assays and did not resulted from knockout of either gene (Figures 5H and S3D).

We then evaluated the growth inhibition effects brought by these two hit combinations by treating OVCAR8-ADR cells with drug pairs. Olaparib (OLA), AZA, seliciclib (SEL), and sirolimus (SIR) were used to target PARP1, DNMT1, CDK2, and FKBP1A, respectively. These drug molecules have been reported to have potent effects on their targets (McClue et al., 2002; Muvarak et al., 2016; Sabers et al., 1995; Wishart et al., 2006; Yang et al., 2017). Our results indicated that OLA and AZA act synergistically to suppress the growth of OVCAR8-ADR cells (Figures 5I–5K) and induce G2 cell cycle arrest (Figure 5L), whereas combined treatment with SEL and SIR had an additive effect that inhibits its growth (Figures 5M–5P). Similar growth inhibition effects were observed when these drug combinations were applied to OVSAHO (Figure S6A) and KURAMOCHI (Figure S6B), two other characterized cell models of HGSOC (Coscia et al., 2016; Domcke et al., 2013). Our results also corroborate the observation that co-administration of the PARP1 inhibitor talazoparib and the DNMT1 inhibitor (gua)decitabine synergistically suppresses tumor growth of other ovarian cancer cells, including OVCAR4, PEO1, and PEO4 (Pulliam et al., 2018), as well as acute myeloid leukemia and breast cancer cells (Muvarak et al., 2016), further suggesting PARP1 + DNMT1 inhibitor combination as an effective therapeutic option for multiple cancer types.

## A CRISPR-Cas9 Screen for Drug Pairs against Parkinson's Disease Toxicity

Our screening approach can be applied to search for effective therapeutic combinations that enhance protection against other disease phenotypes, such as Parkinson's disease (PD)-associated toxicity. We assembled another high-coverage (99.1%) pairwise gRNA library targeting 28 druggable genes whose ablations or matching drug inhibitors have been reported to suppress neuronal toxicity (Figures 6A–6E; Table S2). The library was delivered into SK-N-MC-Cas9 cells via lentiviruses to generate dual gene knockouts, and the cells were then treated with rotenone to induce PD-associated toxicity (Figures 6F and 6G). Barcode abundances for the rotenone-treated and untreated groups were compared to identify enriched gRNA combinations that protect the cells from rotenone-induced toxicity. Based on selection criteria that required a mean $\log_2$ fold-change of more than 0.378 (based on data obtained from two biological replicates with at least 30% more barcode counts in rotenone-treated versus untreated cells) and multiple gRNAs targeting the same gene pair being detected with $p < 0.05$, our genetic screen identified *HSP90B1* + *HDAC2* as the top hit (with six gRNA combinations identified, having an average of a 51.6% increase in barcode counts) that enhances cell survival upon rotenone treatment (Figure 6H; Table S5). The protective effect provided by simultaneous knockout of *HSP90B1* + *HDAC2* was validated in non-pooled assays and was greater than that from knockout of either gene (Figure 6I). We further confirmed the protective effect of the matching drugs (17-(dimethylaminoethylamino)-17-demethoxygeldanamycin [17-DMAG] + vorinostat) for this identified combination. Combined

**Figure 5. A CRISPR-Based Dual-Gene Knockout Screen Identifies Drug Pairs that Inhibit Ovarian Cancer Cell Growth**

(A) Distributions of barcode reads in the plasmid and 9-day post-infection OVCAR8-ADR-Cas9 cell pools. 99.7% (25,201 of 25,281) and 99.0% (25,027 of 25,281) of all expected gRNA combinations were obtained in the plasmid and cell pools, respectively. Most barcoded gRNA combinations were detected within a 5-fold range from the mean barcode reads per combination (highlighted by the shaded areas).

(B) High correlation between barcode representations (normalized barcode counts) within the plasmid pool and infected cell pool indicates efficient lentiviral delivery of the pairwise gRNA library into cells. The horizontal dotted lines in the Bland-Altman plots indicate the 95% limits of agreement.

(C and D) High reproducibility of barcode representations between two biological replicates in cells cultured for 15 days (C) and 21 days (D) post-infection with the pairwise gRNA library. The horizontal dotted lines in the Bland-Altman plots indicate the 95% limits of agreement. The vertical dashed line indicates the threshold of 100 raw barcode counts.

(E) The CV (defined as SD/mean of the fold changes of normalized barcode counts for 21-day versus 15-day cultured cells) was determined for the two biological replicates. Over 99.2% of pairwise gRNA combinations had a CV of less than 1 in the screen.

(F) OVCAR8-ADR-Cas9 cells infected with the barcoded pairwise gRNA library were cultured for 15 and 21 days. Barcode representations within the cell pools were quantified using Illumina HiSeq. The barcoded library vector uses an hH1-gRNA-WT scaffold and hU6-gRNA-v1 scaffold in the first and second expression cassettes, respectively.

(G) A volcano plot for comparing the abundance changes of each barcoded gRNA combination on day 21 versus day 15 post-infection. Hit combinations (*DNMT1* + *PARP1* and *FKBP1A* + *CDK2*) are highlighted in blue and red, respectively. Data were collected from two biological replicates.

(H–J, M, and N) Cell viability, determined by MTT assay, of the indicated gRNA-infected OVCAR8-ADR-Cas9 cells (H) and drug-treated OVCAR8-ADR cells (I, J, M, and N). In (J) and (N), the percentage of growth inhibition was calculated by comparing each drug-treated group with the untreated control. Drug synergy was measured by the Bliss independence model and the highest single agent (HSA) model. The growth-inhibitory effects brought on by treatment with 8 μM of OLA and 1.2 μM of AZA (J) and 5 μM SEL and 0.5 μM SIR (N) were plotted as examples, and the dashed lines indicate the expected drug combination effects based on the Bliss independence model. Data shown are mean ± SD from biological replicates (n = 3 in H, n = 6 in I and J, n = 8 in M and N).

(K and O) Colony formation assay of OLA- and/or AZA-treated (K) and SEL- and/or SIR-treated (O) OVCAR8-ADR cells. The colony numbers and areas were quantified. Data shown are mean ± SD from biological replicates (n = 3).

(L and P) Cell cycle analysis of OLA- and/or AZA-treated (L) and SEL- and/or SIR-treated (P) OVCAR8-ADR cells. The percentage of cells in each cell cycle phase was quantified. Data shown are mean ± SD from biological replicates (n = 3).

Statistical significance in (H)–(P) was analyzed by one-way ANOVA with Tukey's post hoc test. *$p < 0.05$, **$p < 0.01$, and ****$p < 0.0001$; #$p < 0.05$ in (J)–(L), (N), and (O) indicates comparisons with the untreated control. See also Figure S6.

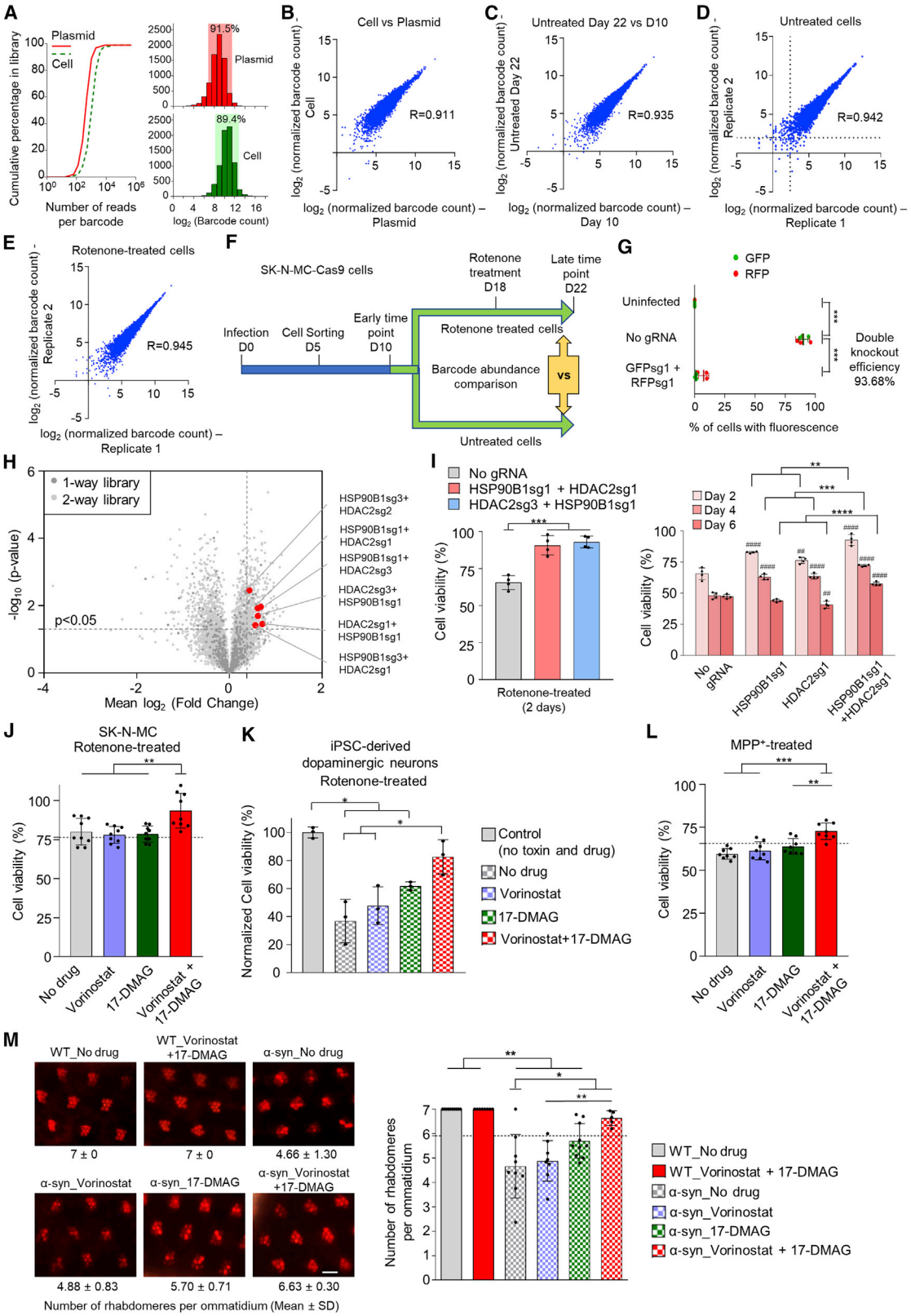


*(legend on next page)*

drug treatment enhanced cell survival against rotenone-induced toxicity compared with single-drug treatments in SK-N-MC cells (Figure 6J) and induced pluripotent stem cell (iPSC)-derived dopaminergic neurons (Figure 6K). In addition, we observed that this drug combination reduced toxicity induced by $MPP^+$ treatment in cultured cells (Figure 6L) and alpha-synuclein expression in transgenic flies (Figure 6M), two other well-characterized models of PD. Our results demonstrate the versatility of our platform for screening therapeutic combinations against different disease phenotypes, including those for alleviating neurodegenerative disease phenotypes.

## DISCUSSION

In summary, we established a CRISPR-based multi-gene knockout screening platform to address the unmet need for rapid identification of effective three-way therapeutic combinations. Pairing drug mechanisms of action to specific genes helps to accelerate identification of effective combinations for directing secondary screens and narrows a vast number of possible combinations down to few top-performing hits for further testing. We demonstrated that systematic characterization of three-way combinations using CRISPR-based screening discovers rare ones with synergistic interactions because most of them showed buffering interactions, and we were able to validate all three screen hits with strong growth inhibition effects and three-way interactions. Our CombiGEM-CRISPR v.2.0 platform has broad utility because it can also be used to identify two-drug regimens that inhibit cancer cell growth and enhance protection against other disease phenotypes, such as PD-associated toxicity, and can be extended to analyze interactions among more than 3 genetic components by using additional engineered promoters and scaffolds for multiplexed CRISPR-based editing (Reis et al., 2019). This platform is also versatile and can be used together with dCas9-based CRISPR interference systems (Qi et al., 2013) to partially lower target gene expressions to mimic drug inhibitor effects and minimize any spurious effects caused by large deletions and genomic rearrangements. This platform could be coupled with other technologies, like single-cell RNA sequencing (RNA-seq), to explore different cell signatures and contribute to generation of druggable gene interaction networks using existing knowledge (Adamson et al., 2016; Bassik et al., 2013; Chow et al., 2019; Du et al., 2017; Han et al., 2017; Shen et al., 2017). The platform presented in this study is easy to implement and will be valuable for perturbing multi-layer genetic networks to understand complex biological systems and design new combination therapies.

## STAR★METHODS

Detailed methods are provided in the online version of this paper and include the following:

- KEY RESOURCES TABLE
- RESOURCE AVAILABILITY
  - Lead Contact
  - Materials Availability
  - Data and Code Availability
- EXPERIMENTAL MODEL AND SUBJECT DETAILS
  - Mice and flies
  - Cell culture and generation of cell lines

**Figure 6. A CRISPR-Based Dual-Gene Knockout Screen Identifies a Drug Combination that Enhances Protection against PD Toxicity**

(A) Distributions of barcode reads in the plasmid and infected SK-N-MC-Cas9 cell pools. 99.1% (7,499 of 7,569) and 98.7% (7,467 of 7,569) of all expected gRNA combinations were obtained in the plasmid and cell pools, respectively. Most barcoded gRNA combinations were detected within a 5-fold range from the mean barcode reads per combination (highlighted by the shaded areas).

(B) High correlation between barcode representations (normalized barcode counts) within the plasmid pool and infected cell pool indicates efficient lentiviral delivery of the pairwise gRNA library into cells.

(C) High correlation between barcode representations within cell pools cultured for 10 and 22 days indicates that the CRISPR-mediated gene knockouts did not result in severe cell death.

(D and E) High reproducibility of barcode representations between two biological replicates in untreated (D) and rotenone-treated (E) cells. The dashed lines in (D) indicate the threshold of 20 raw barcode counts. R is the Pearson correlation coefficient.

(F) SK-N-MC-Cas9 cells infected with the barcoded pairwise gRNA library were treated with rotenone or remained untreated. Barcode representations within the cell pools were quantified using Illumina HiSeq.

(G) Lentiviral delivery of dual-gRNA expression constructs efficiently disrupted multiple target genes in SK-N-MC-Cas9 cells. Flow cytometry was used to measure the percentage of cell populations positive for GFP and RFP fluorescence on day 6 post-infection. Data are mean ± SD; n = 3 biological replicates.

(H) A volcano plot for comparing the abundance changes of each barcoded gRNA combination in rotenone-treated versus untreated cell pools. The hit combination, *HSP90B1* + *HDAC2*, is highlighted in red. Data were collected from two biological replicates.

(I) Cell viability, determined by MTT assay, of the indicated sgRNA-infected SK-N-MC-Cas9 cells in the presence of rotenone. Data shown are mean ± SD (n = 4) from biological replicates, and data in the left and right panels were obtained from the same experiments.

(J and K) Cell viability of the indicated drug-treated SK-N-MC cells (J) and iPSC-derived dopaminergic neurons (K) in the presence of rotenone, determined by MTT assay and DAPI uptake assay, respectively. Data shown are mean ± SD (n = 9 in J, n = 3 in K) from biological replicates.

(L) Cell viability, determined by MTT assay, of the indicated drug-treated SK-N-MC cells in the presence of $MPP^+$. Data shown are mean ± SD (n = 8) from biological replicates.

(M) Quantification of the number of rhabdomeres per ommatidium in WT and alpha-synuclein-expressing flies that were fed the indicated drug(s). Combination of 17-DMAG and vorinostat restored the number of rhabdomeres per ommatidium in alpha-synuclein-expressing *Drosophila* eyes. Representative images show the rhabdomeres of WT and alpha-synuclein-expressing flies that were fed with indicated drug(s). Data are mean ± SD from at least 100 ommatidia of 5–10 flies. The scale bar indicates 20 μm.

Statistical significance in (I)–(M) was analyzed by one-way ANOVA with Tukey's post hoc test. *$p < 0.05$, **$p < 0.01$ and ****$p < 0.0001$ represent significant differences between the indicated samples. In (I), #$p < 0.05$, ##$p < 0.01$, ###$p < 0.001$, and ####$p < 0.0001$ indicate comparisons with the respective no-gRNA controls. A dashed line indicates the expected drug combination effects based on the Bliss independence model.

- METHOD DETAILS
  - Plasmid construction
  - Guide RNA library design and assembly
  - Lentiviral vector generation and transduction
  - Flow cytometry, cell cycle analysis, and cell sorting
  - Sample preparation for barcode reading
  - Barcode sequencing data analysis
  - Cell viability assay and drug interaction analysis
  - Colony formation assay
  - Drug response study in mice
  - Pseudopupil assay
  - RNA-seq
  - GUIDE-seq
- QUANTIFICATION AND STATISTICAL ANALYSIS


## SUPPLEMENTAL INFORMATION

Supplemental Information can be found online at https://doi.org/10.1016/j.celrep.2020.108020.

## ACKNOWLEDGMENTS

We thank members of the Wong lab for helpful discussions. We thank Mr. Guanhua Xun for technical assistance. We thank the Centre for PanorOmic Sciences at LKS Faculty of Medicine, The University of Hong Kong, for providing support with the RNA-seq experiments, flow cytometry analysis, and cell sorting. We also thank the Information Technology Services at The University of Hong Kong for maintaining and providing support with utilizing the High Performance Computing System to process our RNA-seq data. This work was supported by The University of Hong Kong start-up and internal funds, the Hong Kong Research Grants Council (ECS-27105716, GRF-17102218, and TRS-T12-710/16-R), the Innovation and Technology Commission, Hong Kong (ITS/133/18), and the Food and Health Bureau, Hong Kong (HMRF-04151416) (to A.S.L.W.). This work was partially supported by funding from the CUHK Gerald Choa Neuroscience Centre (7105306) (to H.Y.E.C.), the Research Services and Knowledge Transfer Office (MYRG2018-00017-FHS) and Faculty of Health Sciences (FHS collaboration and innovation grants) of the University of Macau, Macao (to K.H.W.), and the Swedish Research Council, Sweden (2016-02830) and National Natural Science Foundation of China, China (81672098) (to Z.Z.). This project has been developed as part of the Ming Wai Lau Centre for Reparative Medicine Associate Member Program. A.S.L.W. is a Ming Wai Lau Centre for Reparative Medicine (MWLC) Associate Member.

## AUTHOR CONTRIBUTIONS

P.Z., B.K.C.C., Y.K.W., and A.S.L.W. conceived the work, designed and performed most of the experiments, and interpreted and analyzed the data. C.T.L.Y., S.Y.L., K.T., and K.H.W. provided support for computational analyses of next-generation sequencing data for the CombiGEM experiments. G.C.G.C., S.S.W.Z., and J.S. provided support for the molecular biology experiments. X.L., C.S.W.T., and L.W.T.C. provided support for the mouse experiments. Y.B., S.Y.L.M., M.Z.Y.C., and Z.Z. provided support for the GUIDE-seq experiments. J.V.K. provided support for gRNA design. H.Y.E.C. provided support for the *Drosophila* experiments. P.Z., B.K.C.C., Y.K.W., G.C.G.C., and A.S.L.W. wrote the paper.

## DECLARATION OF INTERESTS

The authors have filed a patent application based on this work.

Received: January 7, 2020
Revised: June 4, 2020
Accepted: July 20, 2020
Published: August 11, 2020

## REFERENCES

Adamson, B., Norman, T.M., Jost, M., Cho, M.Y., Nunez, J.K., Chen, Y., Villalta, J.E., Gilbert, L.A., Horlbeck, M.A., Hein, M.Y., et al. (2016). A Multiplexed Single-Cell CRISPR Screening Platform Enables Systematic Dissection of the Unfolded Protein Response. Cell *167*, 1867–1882.e21.

Aguirre, A.J., Meyers, R.M., Weir, B.A., Vazquez, F., Zhang, C.Z., Ben-David, U., Cook, A., Ha, G., Harrington, W.F., Doshi, M.B., et al. (2016). Genomic Copy Number Dictates a Gene-Independent Cell Response to CRISPR/Cas9 Targeting. Cancer Discov. *6*, 914–929.

Al-Lazikani, B., Banerji, U., and Workman, P. (2012). Combinatorial drug therapy for cancer in the post-genomic era. Nat. Biotechnol. *30*, 679–692.

Allen, F., Crepaldi, L., Alsinet, C., Strong, A.J., Kleshchevnikov, V., De Angeli, P., Palenikova, P., Khodak, A., Kiselev, V., Kosicki, M., et al. (2018). Predicting the mutations generated by repair of Cas9-induced double-strand breaks. Nat. Biotechnol. Published online November 27, 2018. https://doi.org/10.1038/nbt.4317.

Auluck, P.K., Chan, H.Y., Trojanowski, J.Q., Lee, V.M., and Bonini, N.M. (2002). Chaperone suppression of alpha-synuclein toxicity in a Drosophila model for Parkinson's disease. Science *295*, 865–868.

Baratta, M.G., Schinzel, A.C., Zwang, Y., Bandopadhayay, P., Bowman-Colin, C., Kutt, J., Curtis, J., Piao, H., Wong, L.C., Kung, A.L., et al. (2015). An in-tumor genetic screen reveals that the BET bromodomain protein, BRD4, is a potential therapeutic target in ovarian carcinoma. Proc. Natl. Acad. Sci. USA *112*, 232–237.

Bassik, M.C., Kampmann, M., Lebbink, R.J., Wang, S., Hein, M.Y., Poser, I., Weibezahn, J., Horlbeck, M.A., Chen, S., Mann, M., et al. (2013). A systematic mammalian genetic interaction map reveals pathways underlying ricin susceptibility. Cell *152*, 909–922.

Bliss, C. (1939). The toxicity of poisons applied jointly. Ann. Appl. Biol. *26*, 585–615.

Borisy, A.A., Elliott, P.J., Hurst, N.W., Lee, M.S., Lehar, J., Price, E.R., Serbedzija, G., Zimmermann, G.R., Foley, M.A., Stockwell, B.R., and Keith, C.T. (2003). Systematic discovery of multicomponent therapeutics. Proc. Natl. Acad. Sci. USA *100*, 7977–7982.

Bowtell, D.D. (2010). The genesis and evolution of high-grade serous ovarian cancer. Nat. Rev. Cancer *10*, 803–808.

Bozic, I., Reiter, J.G., Allen, B., Antal, T., Chatterjee, K., Shah, P., Moon, Y.S., Yaqubie, A., Kelly, N., Le, D.T., et al. (2013). Evolutionary dynamics of cancer in response to targeted combination therapy. eLife *2*, e00747.

Briner, A.E., Donohoue, P.D., Gomaa, A.A., Selle, K., Slorach, E.M., Nye, C.H., Haurwitz, R.E., Beisel, C.L., May, A.P., and Barrangou, R. (2014). Guide RNA functional modules direct Cas9 activity and orthogonality. Mol. Cell *56*, 333–339.

Choi, G.C.G., Zhou, P., Yuen, C.T.L., Chan, B.K.C., Xu, F., Bao, S., Chu, H.Y., Thean, D., Tan, K., Wong, K.H., et al. (2019). Combinatorial mutagenesis en masse optimizes the genome editing activities of SpCas9. Nat. Methods *16*, 722–730.

Chow, R.D., Wang, G., Ye, L., Codina, A., Kim, H.R., Shen, L., Dong, M.B., Errami, Y., and Chen, S. (2019). In vivo profiling of metastatic double knockouts through CRISPR-Cpf1 screens. Nat. Methods *16*, 405–408.

Cokol, M., Kuru, N., Bicak, E., Larkins-Ford, J., and Aldridge, B.B. (2017). Efficient measurement and factorization of high-order drug interactions in *Mycobacterium tuberculosis*. Sci. Adv. *3*, e1701881.

Cokol-Cakmak, M., Bakan, F., Cetiner, S., and Cokol, M. (2018). Diagonal Method to Measure Synergy Among Any Number of Drugs. J. Vis. Exp. (*136*), 57713.

Coscia, F., Watters, K.M., Curtis, M., Eckert, M.A., Chiang, C.Y., Tyanova, S., Montag, A., Lastra, R.R., Lengyel, E., and Mann, M. (2016). Integrative proteomic profiling of ovarian cancer cell lines reveals precursor cell associated proteins and functional status. Nat. Commun. *7*, 12645.

Dang, Y., Jia, G., Choi, J., Ma, H., Anaya, E., Ye, C., Shankar, P., and Wu, H. (2015). Optimizing sgRNA structure to improve CRISPR-Cas9 knockout efficiency. Genome Biol. *16*, 280.

Dobin, A., Davis, C.A., Schlesinger, F., Drenkow, J., Zaleski, C., Jha, S., Batut, P., Chaisson, M., and Gingeras, T.R. (2013). STAR: ultrafast universal RNA-seq aligner. Bioinformatics *29*, 15–21.

Doench, J.G. (2018). Am I ready for CRISPR? A user's guide to genetic screens. Nat. Rev. Genet. *19*, 67–80.

Doench, J.G., Fusi, N., Sullender, M., Hegde, M., Vaimberg, E.W., Donovan, K.F., Smith, I., Tothova, Z., Wilen, C., Orchard, R., et al. (2016). Optimized sgRNA design to maximize activity and minimize off-target effects of CRISPR-Cas9. Nat. Biotechnol. *34*, 184–191.

Domcke, S., Sinha, R., Levine, D.A., Sander, C., and Schultz, N. (2013). Evaluating cell lines as tumour models by comparison of genomic profiles. Nat. Commun. *4*, 2126.

Du, D., Roguev, A., Gordon, D.E., Chen, M., Chen, S.H., Shales, M., Shen, J.P., Ideker, T., Mali, P., Qi, L.S., and Krogan, N.J. (2017). Genetic interaction mapping in mammalian cells using CRISPR interference. Nat. Methods *14*, 577–580.

Engler, C., Kandzia, R., and Marillonnet, S. (2008). A one pot, one step, precision cloning method with high throughput capability. PLoS ONE *3*, e3647.

Fabregat, A., Sidiropoulos, K., Viteri, G., Forner, O., Marin-Garcia, P., Arnau, V., D'Eustachio, P., Stein, L., and Hermjakob, H. (2017). Reactome pathway analysis: a high-performance in-memory approach. BMC Bioinformatics *18*, 142.

Gholami, A.M., Hahne, H., Wu, Z., Auer, F.J., Meng, C., Wilhelm, M., and Kuster, B. (2013). Global proteome analysis of the NCI-60 cell line panel. Cell Rep. *4*, 609–620.

Gibson, D.G., Young, L., Chuang, R.Y., Venter, J.C., Hutchison, C.A., 3rd, and Smith, H.O. (2009). Enzymatic assembly of DNA molecules up to several hundred kilobases. Nat. Methods *6*, 343–345.

Grevet, J.D., Lan, X., Hamagami, N., Edwards, C.R., Sankaranarayanan, L., Ji, X., Bhardwaj, S.K., Face, C.J., Posocco, D.F., Abdulmalik, O., et al. (2018). Domain-focused CRISPR screen identifies HRI as a fetal hemoglobin regulator in human erythroid cells. Science *361*, 285–290.

Han, K., Jeng, E.E., Hess, G.T., Morgens, D.W., Li, A., and Bassik, M.C. (2017). Synergistic drug combinations for cancer identified in a CRISPR screen for pairwise genetic interactions. Nat. Biotechnol. *35*, 463–474.

Honma, K., Iwao-Koizumi, K., Takeshita, F., Yamamoto, Y., Yoshida, T., Nishio, K., Nagahara, S., Kato, K., and Ochiya, T. (2008). RPN2 gene confers docetaxel resistance in breast cancer. Nat. Med. *14*, 939–948.

Huang, W., Sherman, B.T., and Lempicki, R.A. (2009). Systematic and integrative analysis of large gene lists using DAVID bioinformatics resources. Nat. Protoc. *4*, 44–57.

Kosicki, M., Tomberg, K., and Bradley, A. (2018). Repair of double-strand breaks induced by CRISPR-Cas9 leads to large deletions and complex rearrangements. Nat. Biotechnol. *36*, 765–771.

Liao, Y., Smyth, G.K., and Shi, W. (2019). The R package Rsubread is easier, faster, cheaper and better for alignment and quantification of RNA sequencing reads. Nucleic Acids Res. *47*, e47.

Ma, H., Wu, Y., Dang, Y., Choi, J.G., Zhang, J., and Wu, H. (2014). Pol III Promoters to Express Small RNAs: Delineation of Transcription Initiation. Mol. Ther. Nucleic Acids *3*, e161.

McClue, S.J., Blake, D., Clarke, R., Cowan, A., Cummings, L., Fischer, P.M., MacKenzie, M., Melville, J., Stewart, K., Wang, S., et al. (2002). In vitro and in vivo antitumor properties of the cyclin dependent kinase inhibitor CYC202 (R-roscovitine). Int. J. Cancer *102*, 463–468.

Munoz, D.M., Cassiani, P.J., Li, L., Billy, E., Korn, J.M., Jones, M.D., Golji, J., Ruddy, D.A., Yu, K., McAllister, G., et al. (2016). CRISPR Screens Provide a Comprehensive Assessment of Cancer Vulnerabilities but Generate False-Positive Hits for Highly Amplified Genomic Regions. Cancer Discov. *6*, 900–913.

Muvarak, N.E., Chowdhury, K., Xia, L., Robert, C., Choi, E.Y., Cai, Y., Bellani, M., Zou, Y., Singh, Z.N., Duong, V.H., et al. (2016). Enhancing the Cytotoxic Effects of PARP Inhibitors with DNA Demethylating Agents - A Potential Therapy for Cancer. Cancer Cell *30*, 637–650.

Najm, F.J., Strand, C., Donovan, K.F., Hegde, M., Sanson, K.R., Vaimberg, E.W., Sullender, M.E., Hartenian, E., Kalani, Z., Fusi, N., et al. (2018). Orthologous CRISPR-Cas9 enzymes for combinatorial genetic screens. Nat. Biotechnol. *36*, 179–189.

Pulliam, N., Fang, F., Ozes, A.R., Tang, J., Adewuyi, A., Keer, H., Lyons, J., Baylin, S.B., Matei, D., Nakshatri, H., et al. (2018). An Effective Epigenetic-PARP Inhibitor Combination Therapy for Breast and Ovarian Cancers Independent of BRCA Mutations. Clin. Cancer Res. *24*, 3163–3175.

Qi, L.S., Larson, M.H., Gilbert, L.A., Doudna, J.A., Weissman, J.S., Arkin, A.P., and Lim, W.A. (2013). Repurposing CRISPR as an RNA-guided platform for sequence-specific control of gene expression. Cell *152*, 1173–1183.

Rau, A., Gallopin, M., Celeux, G., and Jaffrézic, F. (2013). Data-based filtering for replicated high-throughput transcriptome sequencing experiments. Bioinformatics *29*, 2146–2152.

Reinhold, W.C., Sunshine, M., Liu, H., Varma, S., Kohn, K.W., Morris, J., Doroshow, J., and Pommier, Y. (2012). CellMiner: a web-based suite of genomic and pharmacologic tools to explore transcript and drug patterns in the NCI-60 cell line set. Cancer Res. *72*, 3499–3511.

Reis, A.C., Halper, S.M., Vezeau, G.E., Cetnar, D.P., Hossain, A., Clauer, P.R., and Salis, H.M. (2019). Simultaneous repression of multiple bacterial genes using nonrepetitive extra-long sgRNA arrays. Nat. Biotechnol. *37*, 1294–1301.

Ritchie, M.E., Phipson, B., Wu, D., Hu, Y., Law, C.W., Shi, W., and Smyth, G.K. (2015). limma powers differential expression analyses for RNA-sequencing and microarray studies. Nucleic Acids Res. *43*, e47.

Robinson, M.D., McCarthy, D.J., and Smyth, G.K. (2010). edgeR: a Bioconductor package for differential expression analysis of digital gene expression data. Bioinformatics *26*, 139–140.

Sabers, C.J., Martin, M.M., Brunn, G.J., Williams, J.M., Dumont, F.J., Wiederrecht, G., and Abraham, R.T. (1995). Isolation of a protein target of the FKBP12-rapamycin complex in mammalian cells. J. Biol. Chem. *270*, 815–822.

Schneider, C.A., Rasband, W.S., and Eliceiri, K.W. (2012). NIH Image to ImageJ: 25 years of image analysis. Nat. Methods *9*, 671–675.

Shalem, O., Sanjana, N.E., Hartenian, E., Shi, X., Scott, D.A., Mikkelson, T., Heckl, D., Ebert, B.L., Root, D.E., Doench, J.G., and Zhang, F. (2014). Genome-scale CRISPR-Cas9 knockout screening in human cells. Science *343*, 84–87.

Shen, J.P., Zhao, D., Sasik, R., Luebeck, J., Birmingham, A., Bojorquez-Gomez, A., Licon, K., Klepper, K., Pekin, D., Beckett, A.N., et al. (2017). Combinatorial CRISPR-Cas9 screens for de novo mapping of genetic interactions. Nat. Methods *14*, 573–576.

Shen, M.W., Arbab, M., Hsu, J.Y., Worstell, D., Culbertson, S.J., Krabbe, O., Cassa, C.A., Liu, D.R., Gifford, D.K., and Sherwood, R.I. (2018). Predictable and precise template-free CRISPR editing of pathogenic variants. Nature *563*, 646–651.

Shin, H.Y., Wang, C., Lee, H.K., Yoo, K.H., Zeng, X., Kuhns, T., Yang, C.M., Mohr, T., Liu, C., and Hennighausen, L. (2017). CRISPR/Cas9 targeting events cause complex deletions and insertions at 17 sites in the mouse genome. Nat. Commun. *8*, 15464.

Tsai, S.Q., Zheng, Z., Nguyen, N.T., Liebers, M., Topkar, V.V., Thapar, V., Wyvekens, N., Khayter, C., Iafrate, A.J., Le, L.P., et al. (2015). GUIDE-seq enables genome-wide profiling of off-target cleavage by CRISPR-Cas nucleases. Nat. Biotechnol. *33*, 187–197.

Vidigal, J.A., and Ventura, A. (2015). Rapid and efficient one-step generation of paired gRNA CRISPR-Cas9 libraries. Nat. Commun. *6*, 8083.

Wishart, D.S., Knox, C., Guo, A.C., Shrivastava, S., Hassanali, M., Stothard, P., Chang, Z., and Woolsey, J. (2006). DrugBank: a comprehensive resource for in silico drug discovery and exploration. Nucleic Acids Res. *34*, D668–D672.

Wong, S.L., Chan, W.M., and Chan, H.Y. (2008). Sodium dodecyl sulfate-insoluble oligomers are involved in polyglutamine degeneration. FASEB J. *22*, 3348–3357.

Wong, A.S., Choi, G.C., Cheng, A.A., Purcell, O., and Lu, T.K. (2015). Massively parallel high-order combinatorial genetics in human cells. Nat. Biotechnol. *33*, 952–961.

Wong, A.S., Choi, G.C., Cui, C.H., Pregernig, G., Milani, P., Adam, M., Perli, S.D., Kazer, S.W., Gaillard, A., Hermann, M., et al. (2016a). Multiplexed barcoded CRISPR-Cas9 screening enabled by CombiGEM. Proc. Natl. Acad. Sci. USA *113*, 2544–2549.

Wong, A.S., Choi, G.C., and Lu, T.K. (2016b). Deciphering Combinatorial Genetics. Annu. Rev. Genet. *50*, 515–538.

Wood, K., Nishida, S., Sontag, E.D., and Cluzel, P. (2012). Mechanism-independent method for predicting response to multidrug combinations in bacteria. Proc. Natl. Acad. Sci. USA *109*, 12254–12259.

Xu, L., Zhao, L., Gao, Y., Xu, J., and Han, R. (2017). Empower multiplex cell and tissue-specific CRISPR-mediated gene manipulation with self-cleaving ribozymes and tRNA. Nucleic Acids Res. *45*, e28.

Yang, L., Zhang, Y., Shan, W., Hu, Z., Yuan, J., Pi, J., Wang, Y., Fan, L., Tang, Z., Li, C., et al. (2017). Repression of BET activity sensitizes homologous recombination-proficient cancers to PARP inhibition. Sci. Transl. Med. *9*, eaal1645.

Zimmer, A., Katzir, I., Dekel, E., Mayo, A.E., and Alon, U. (2016). Prediction of multidimensional drug dose responses based on measurements of drug pairs. Proc. Natl. Acad. Sci. USA *113*, 10442–10447.

## STAR★METHODS

### KEY RESOURCES TABLE

| REAGENT or RESOURCE | SOURCE | IDENTIFIER |
|---|---|---|
| Antibodies | | |
| Phospho-Histone H3 (Ser10) Antibody | Cell Signaling Technology | Cat# 9701; RRID:AB_331535 |
| Chemicals, Peptides, and Recombinant Proteins | | |
| Zeocin | Life Technologies | Cat#R25001 |
| FuGene HD transfection reagent | Promega | Cat#E2312 |
| Polybrene | Sigma | Cat#TR-1003-G |
| Propidium iodide | Invitrogen | Cat#BMS500PI |
| Rotenone | Abcam | Cat#ab143145 |
| MPP+ | Abcam | Cat#ab144783 |
| Azacitidine | LC Laboratories | Cat#A-5959 |
| Olaparib | LC Laboratories | Cat#O-9201 |
| Sirolimus | LC Laboratories | Cat#R-5000 |
| Seliciclib | LC Laboratories | Cat#R-1234 |
| Lapatinib | LC Laboratories | Cat#L-4899 |
| Erlotinib | LC Laboratories | Cat#E4007 |
| Vorinostat | LC Laboratories | Cat#V-8477 |
| Fludarabine | Cayman Chemical Company | Cat#14128 |
| 17-DMAG | InvivoGen | Cat#ant-dgl-25 |
| Critical Commercial Assays | | |
| Quant-iT PicoGreen dsDNA Assay kit | Life Technologies | Cat#P11496 |
| Kapa HiFi Hotstart Ready-mix | Kapa Biosystems | Cat#KK2602 |
| Agencourt AMPure XP beads | Beckman Coulter Genomics | Cat#A63881 |
| Kapa SYBR Fast qPCR Master Mix | Kapa Biosystems | Cat#KK4600 |
| Kapa HyperPlus Kit | Roche | Cat#KK8514 |
| Deoxynucleotide (dNTP) Solution Mix | New England Biolabs | Cat#N0447L |
| SPRIselect | Beckman Coulter | Cat#B23318 |
| PlatinumTM Taq DNA Polymerase | Invitrogen | Cat#10966034 |
| CollibriTM Library Quantification Kit | Invitrogen | Cat#A38524100 |
| Deposited Data | | |
| Reads for three-way combinatorial CRISPR-Cas9 screen performed in OVCAR8-ADR-Cas9 cells (Related to Figure 3) | This study | NCBI GEO (GSE154112) |
| Reads for pairwise CRISPR-Cas9 screen performed in in OVCAR8-ADR-Cas9 cells (Related to Figure 5) | This study | NCBI GEO (GSE154112) |
| Reads for pairwise CRISPR-Cas9 screen performed in SK-N-MC-Cas9 cells (Related to Figure 6) | This study | NCBI GEO (GSE154112) |
| RNA-seq read counts in OVCAR8-ADR cells treated with drug combinations (Related to Figure S4A) | This study | NCBI GEO (GSE154112) |
| GUIDE-seq reads (Related to Figure S3C) | This study | European Nucleotide Archive PRJEB39350 |
| Experimental Models: Cell Lines | | |
| Human: HEK293T (female) | ATCC | CRL-3216 |
| Human: SK-N-MC (female) | ATCC | HTB-10 |
| Human: OVCAR8-ADR (female) | Honma et al., 2008 | N/A |
| Human: KURAMOCHI (female) | JCRB | JCRB0098 |

(*Continued on next page*)

*Continued*

| REAGENT or RESOURCE | SOURCE | IDENTIFIER |
|---|---|---|
| Human: OVSAHO (female) | JCRB | JCRB1046 |
| Human: iPSC-derived dopaminergic neurons | TGD life company limited | T03.1a-AW |
| Experimental Models: Organisms/Strains | | |
| BALB/cAnN-nu mice | Charles River Lab | N/A |
| GMR-GAL4 (*Drosophila* strain) | FlyBase | FBtp0018010 |
| UAS-α-synuclein (*Drosophila* strain) | FlyBase | FBtp0012468 |
| Oligonucleotides | | |
| All gRNAs used are listed in Table S3 | This study | N/A |
| Recombinant DNA | | |
| All plasmid constructs are listed in Table S6 | This study | N/A |
| Software and Algorithms | | |
| inDelphi | Shen et al., 2018 | http://indelphi.giffordlab.mit.edu/ |
| FORECasT | Allen et al., 2018 | https://github.com/felicityallen/SelfTarget |
| FlowJo v10.5.3 | Becton Dickinson | N/A |
| R package DescTools | N/A | https://cran.r-project.org/web/packages/DescTools/index.html |
| ImageJ | Schneider et al., 2012 | https://imagej.nih.gov/ij/ |
| STAR aligner v2.7 | Dobin et al., 2013 | https://github.com/alexdobin/STAR |
| R package Rsubread | Liao et al., 2019 | 10.18129/B9.bioc.Rsubread |
| R packages EdgeR | Robinson et al., 2010 | 10.18129/B9.bioc.edgeR |
| limma | Ritchie et al., 2015 | 10.18129/B9.bioc.limma |
| HTSFilter | Rau et al., 2013 | 10.18129/B9.bioc.HTSFilter |
| DAVID web tools | Huang et al., 2009 | https://david.ncifcrf.gov/ |
| Reactome pathway database | Fabregat et al., 2017 | https://reactome.org/ |
| GraphPad Prism 7 | GraphPad Software | N/A |

## RESOURCE AVAILABILITY

### Lead Contact

Further information and requests for resources and reagents should be directed to and will be fulfilled by the Lead Contact, Alan S. L. Wong (aslw@hku.hk).

### Materials Availability

Plasmids generated in this study have been deposited to Addgene: pAWp92, #157975; pAWp28-v1 scaffold, #157976; pAWp100, #157977; pAWp102-v2 scaffold, #157978; and pAWp40, #157980.

### Data and Code Availability

The sequencing data generated during this study are available at NCBI GEO under accession GSE154112 and European Nucleotide Archive PRJEB39350. The pipeline and codes for analyzing CombiGEM-CRISPR v.2.0 data are available on https://github.com/AWHKU/CombiPIPE.

## EXPERIMENTAL MODEL AND SUBJECT DETAILS

### Mice and flies

Female BALB/cAnN-nu mice were purchased from Charles River Lab, USA. Six-week-old mice were used for the drug response study. All procedures were carried out with the approval of the Ethics Committee of University of Hong Kong and performed in compliance with the institutional guidelines. Wild-type and transgenic *Drosophila* strains carrying *gmr-GAL4* and *UAS-α-syn* (Auluck et al., 2002) were used in the pseudopupil assay.

### Cell culture and generation of cell lines

HEK293T (female) and SK-N-MC (female) cells were obtained from American Type Culture Collection (ATCC). OVCAR8-ADR (female) cells were a gift from T. Ochiya (Japanese National Cancer Center Research Institute, Japan) (Honma et al., 2008). The identity of the OVCAR8-ADR cells was confirmed by a cell line authentication test (Genetica DNA Laboratories). KURAMOCHI (female) and OVSAHO (female) cells were obtained from Japanese Collection of Research Bioresources (JCRB) Cell Bank. iPSC-derived dopaminergic neurons were obtained from TGD Life Company Limited. OVCAR8-ADR-Cas9 and SK-N-MC-Cas9 cells were generated by transducing pAWp30 (Addgene, 73857) into the OVCAR8-ADR and SK-N-MC cells, respectively, followed by selection using zeocin (Life Technologies) for stable Cas9-integrated cells. The *Streptococcus pyogenes* Cas9 was used in this study. OVCAR8-ADR reporter cells that stably express RFP and GFP were generated by transducing the cells with pAWp9, followed by sorting based on GFP and RFP signals. The reporter cells were then infected with pAWp30 to stably integrate Cas9 after zeocin selection. HEK293T and S-N-MC cells were cultured in DMEM supplemented with 10% FBS and 1 X antibiotic-antimycotic (Life Technologies) at 37°C with 5% $CO_2$. KURAMOCHI, OVSAHO, and OVCAR8-ADR cells were cultured in RPMI 1640 supplemented with 10% FBS and 1 X antibiotic-antimycotic at 37°C with 5% $CO_2$. Cells were checked for mycoplasma contamination every three or four months and were never tested positive.

## METHOD DETAILS

### Plasmid construction

The vectors used in this study (Table S6) were generated by standard molecular cloning strategies, including PCR, oligo annealing, restriction enzyme digestion, ligation, and Gibson assembly. Custom oligonucleotides were purchased from Genewiz. Vectors were transformed into *E. coli* strain *DH5α* competent cells and selected with ampicillin (100 μg/ml, USB) or carbenicillin (50 μg/ml, Teknova). DNA was extracted and purified by Plasmid Mini (Takara and Tiangen) or Midi preparation (QIAGEN) kits. Sequences of the vectors were verified with Sanger sequencing.

To construct storage vectors with mouse U6 (mU6)- and human H1 (hH1) promoter-gRNA WT scaffold sequences, the promoter sequences were amplified from mouse and human genomic DNAs, respectively, and cloned into the vector backbone of pAWp28 (Addgene, 73850). pAWp28 is the storage vector with human U6 (hU6) promoter-gRNA WT scaffold sequence. Storage vectors with hU6-gRNA v1 scaffold and mU6-gRNA v2 scaffold were created by PCR-based mutagenesis. To drive gRNA expression to target the gene of interest, oligo pairs with gRNA target sequences were synthesized, annealed, and cloned into BbsI-digested storage vectors by T4 DNA ligase (New England Biolabs). To generate lentiviral vectors for expression of single gRNA targeting *GFP*, *RFP*, and *BFP* gene, the gRNA expression cassettes were released from the storage vectors by digestion with BglII and EcoRI enzymes (Thermo Fisher Scientific) and cloned into pAWp9 vector (Addgene, 73851) using ligation via the compatible stick ends generated by digestion of the vector with BamHI and EcoRI enzymes (Thermo Fisher Scientific). To build lentiviral vectors for expression of multiple gRNAs targeting the fluorescent proteins, the second gRNA expression cassette with hU6-gRNA-v1 (or WT) scaffold was released from the storage vector by digestion with BglII and EcoRI enzymes, and ligated into the BamHI- and EcoRI- digested storage vector containing the first gRNA expression cassette with hH1-gRNA-WT scaffold. Similarly, the third gRNA expression cassette with mU6-gRNA-v2 (or WT) scaffold was released from the storage vector by digestion and ligated into the storage vector harboring the first and second gRNA expression cassettes. Lentiviral vectors were then generated by amplifying the pairwise or three-way gRNA expression cassettes from the storage vector by PCR, and cloned into the SbfI-digested pFUGW vector backbone (pAWp40) by Gibson assembly.

### Guide RNA library design and assembly

The gRNAs used in this study were designed based on GPP sgRNA Designer (Table S3). For the pairwise gRNA libraries, three gRNAs were selected per target gene based on the following criteria: 1) on-target efficacy scores are > 0.6; 2) off-target ranks are < 100; and 3) target sites are within 5%–65% of the protein-coding sequence. gRNA sequences containing BamHI, EcoRI, BglII, and MfeI digestion sites were excluded to avoid incompatibility with CombiGEM. For the three-wise combinatorial gRNA library, two gRNAs were selected per target gene using the same criteria, except that their on-target efficacy scores are all > 0.64. inDelphi and FORECasT were applied to predict the frameshift rate of gRNA. The gRNA sequences were inputted into BLAST to extract the 70-nucleotide context sequences of the gRNAs. The PAM sequence index were located in the 70-nt sequences and were inputted alongside with the context sequence into inDelphi and FORECasT, which were downloaded from GitHub. The K562 cell line was the prediction model used in inDelphi, and the output frameshift scores are extracted from the "Frameshift frequency" option. The output summary file from FORECasT was inputted into a Python code calculating the predicted frameshift frequency by summing up the percentage of the target frameshift categories that are not multiples of three then dividing the sum by 10.

To assemble the gRNA libraries (Figure S1B), oligo pairs with the gRNA target sequence, two BbsI restriction digestion sites, and a unique 8-bp barcode were annealed, pooled at an equal molar ratio, and cloned into storage vector backbones containing the hH1, hU6, and mU6 promoter sequences (pAWp92, AWp28, and pAWp100, respectively). The gRNA scaffold sequences (WT, v1, and v2) were then inserted into the vectors to create three pooled libraries of barcoded single gRNA expression cassette. The combinatorial gRNA libraries were assembled using the CombiGEM-CRISPR method (Wong et al., 2016a). The first pool of inserts was released from the storage vector containing the hH1-gRNA-WT scaffold by digestion with BglII and MfeI enzymes and ligated

into the BamHI- and EcoRI- digested pAWp12 (Addgene, 72732) to generate the barcoded single gRNA library in a lentiviral vector. Then, the second pool of inserts was released from the storage vector containing the hU6-gRNA-v1 scaffold by digestion and ligated into the lentiviral vector containing the first gRNA expression cassette to generate the barcoded pairwise gRNA library. Similarly, the third pool of inserts was released from the storage vector containing the mU6-gRNA-v2 scaffold and inserted into the lentiviral vector containing the two gRNA expression cassettes to generate the barcoded three-way combinatorial gRNA library. The three-way combinatorial gRNA library was delivered into OVCAR8-ADR cells using lentiviruses, and Sanger sequencing analysis was performed on genomic DNA extracted from single cell-derived clones and confirmed the majority of assembled barcoded gRNA constructs (7 out of 8 colonies) harbored the expected gRNA target sequences. To construct the individual combinatorial gRNA vectors used in the validation experiments, the same assembly strategy was used, except that the annealed oligo pairs were not pooled.

### Lentiviral vector generation and transduction

The second-generation lentiviral vector system was used in this study. HEK293T cells were transfected by FuGene HD transfection reagent (Promega) according to manufacturer's instructions in 6-well plate, with 0.5 μg of pCMV-VSV-G, 1 μg of pCMV-dR8.2-dvpr, and 0.5 μg of the respective lentiviral vector per well. Lentivirus-containing supernatants were collected at 48 and 72 hr post-transfection, which are then combined and filtered by 0.45 μm polyethersulfone membrane (Pall). For routine transduction, we applied 300 μL of the filtered supernatant to one well of 12-well plate in the presence of 8 μg/ml polybrene (Sigma), with cell confluence at about 30%. For library transduction, Cas9-expressing cells were seeded onto 150-mm culture dishes at confluence about 50% with the cell number roughly equals 400-fold representation of the library size, and were transduced by the viruses at a multiplicity of infection (MOI) of ~0.3-0.5, to ensure most cells were infected with just one virion.

### Flow cytometry, cell cycle analysis, and cell sorting

To prepare samples for flow cytometry, cells were trypsinized and resuspended in FACS buffer (PBS with 2% FBS). BD LSR Fortessa analyzer (Becton Dickinson) was used to detect the signal of TurboRFP, EGFP, and mTagBFP by 561 nm yellow-green laser (610/20 nm), 488 nm blue laser (530/30 nm), and 405 nm violet laser (450/50 nm), respectively. For cell cycle analysis, cells were fixed by ice-cold 70% ethanol at 4°C for 1 hr, and then rehydrated by replacing the ethanol with PBS for 15 min at room temperature. To remove RNAs, RNase A (10 mg/ml) was added to the cells and incubated at 37°C for 15 min. Genomic DNA contents were stained by propidium iodide (PI; Invitrogen) for 1 hr at room temperature in dark. Signal was detected by 561 nm yellow-green laser (586/15 nm) using a BD LSR Fortessa analyzer. FlowJo software (v10.5.3, Becton Dickinson) was used for data analysis. For cell sorting, samples were prepared similarly as for FACS analysis, except that FACS buffer was supplemented with 2 X antibiotic-antimycotic. BD Influx cell sorter (Becton Dickinson) equipped with 100-μm nozzle (24 psi with a frequency of 39.2 kHz) was used. GFP-positive cells were detected by 488 nm blue laser (530/40 nm) and sorted using 1.0 Drop Pure mode. For cells being infected with the screening libraries, the 1%–2% cells that had the strongest GFP signals were not collected to minimize the chance of acquiring cells that were infected with more than a single virion. At least 100-fold more cells than the library size were collected.

### Sample preparation for barcode reading

For library-transduced cell pool, genomic DNA was extracted from cells with DNeasy Blood and Tissue kit (QIAGEN) and quantified by Quant-iT PicoGreen dsDNA Assay kit (Life Technologies). To extract the 298-bp barcode-containing fragments, 0.5 ng of library plasmid DNA and 800 ng of genomic DNA per 50 μl of PCR reaction were used for PCR amplification using Kapa HiFi Hotstart Readymix (Kapa Biosystems). The forward and reverse primers used were 5′-GGATCCGCAACGGAATTC-3′ and 5′-GGTTGCGTCAG CAAACACAG-3′. The PCR amplification was kept at the exponential phase to minimize PCR bias. To ensure sufficient library coverage amplified from the genomic DNA, 20 and 10 PCR reactions were performed for the pairwise libraries used in studying ovarian cancer and Parkinson's disease, respectively, and 30 PCR reactions were performed for three-way combinatorial library. Illumina adapters and sequencing indices were then added to the amplicons by performing PCR using Kapa HiFi Hotstart Ready-mix. The forward and reverse primers used were 5′-CAAGCAGAAGACGGCATACGAGATGTGACTGGAGTTCAGACGTGTGCTCTTCC GATCTGGTTGCGTCAGCAAACACAG-3′ and 5′-AATGATACGGCGACCACCGAGATCTACACTCTTTCCCTACACGACGCTCTTCC GATCTNNNNNNNN($N_{1-4}$)GGATCCGCAACGGAATTC-3′, where NNNNNNNN denotes a specific indexing barcode assigned for each experimental sample and ($N_{1-4}$) indicates the 1 to 4 nucleotides added to increase the diversity of the sequencing library. The final amplicons were purified by two rounds of size selection using a 1:0.5 and 1:0.95 ratio of Agencourt AMPure XP beads (Beckman Coulter Genomics). Quantity and quality of samples were measured by real-time PCR using Kapa SYBR Fast qPCR Master Mix (Kapa Biosystems) with primer pair 5′-AATGATACGGCGACCACCGA-3′ and 5′-CAAGCAGAAGACGGCATACGA-3′, and analyzed using a high-sensitivity DNA chip (Agilent) on an Agilent 2100 Bioanalyzer.

### Barcode sequencing data analysis

Barcode reads were processed from the sequencing data and normalized to count per million reads for comparison among samples. The normalized barcode counts for each gRNA combination in the cell pools were compared to the ones for dummy control gRNA combination within each sample to generate a $\log_2$-transformed fold change. To improve data reliability, combinations that had a raw barcode read of < 100 in the early time point samples from the ovarian cancer studies were excluded (Figures 3C and 5C). Combinations that had a raw barcode read of < 20 in the untreated samples from the Parkinson's disease study were filtered out as there

were fewer total reads (Figure 6D). Also, only combinations that contain gRNAs targeting different genes, and had a coefficient of variation (CV) of < 1 are included in the analysis (Figures 3E and 5E). Overall, 97.3% (22,921 out of 23,556 combinations) and 79.1% (21,172 out of 26,782 combinations) of the pairwise and three-way combinations are included, respectively, in the ovarian cancer study. 96.7% (6,878 out of 7,108 combinations) of the pairwise combinations are included in the Parkinson's disease study. In the ovarian cancer studies, gRNA combinations with $\log_2$ fold-change of $< -1$ are listed in Table S5. In the Parkinson's disease study, gRNA combinations with $\log_2$ fold-change > 0.378 (~30% increase) and $p < 0.05$ are listed in Table S5. To identify synergistic three-way combinations, the gRNA combinations targeting three non-redundant genes with a coefficient of variance < 1 were grouped into the total of 455 unique three-gene targeting combinations. The R package DescTools was used to perform Dunnett's test, where the three-way combinations served as the control and being compared to the two-gene and single-gene targeting combinations (6 comparisons in total). To measure genetic interactions, a scoring system similar to one we previously described was applied (Wong et al., 2015). Genetic interaction (GI) scores were calculated by subtracting the expected fold change of the triple-gene knockout, which is estimated by the sum of respective double- and single- gene knockouts' fold changes, by the observed fold change of the triple-gene knockout, where a negative GI score indicates genetic synergy in this study. GI scores calculated for a given three-way combination represent the interaction between the third gene with the remaining two genes in combination. The $GI_3$ score for a three-way combination was calculated based on the geometric mean of the three GI scores. The potentially synergistic gene combinations were selected through the adjusted P value threshold of < 0.05 in all 6 comparisons from the Dunnett's test, a mean $\log_2$ fold change of $< -1$, and $GI_3$ scores of $< -0.2$ (also with GI scores of $< -0.14$ in all 3 possible permutations ("A,B" + "C," "A,C" + "B," "B,C" + "A") for the same three-way combination).

### Cell viability assay and drug interaction analysis

1,500 OVCAR8-ADR cells were seeded onto one well of a 96-well plate one day prior to drug treatment. 4,800 SK-N-MC cells were seeded onto one well of a 96-well plate and were pre-treated with the drug(s) for 72 hours, followed by adding rotenone (Abcam, ab143145) or $MPP^+$ (Abcam, ab144783) to induce toxicity. Drugs were applied at indicated doses. Azacitidine (A-5959), olaparib (O-9201), sirolimus (R-5000), seliciclib (R-1234), lapatinib (L-4899), erlotinib (E4007), and vorinostat (V-8477) were purchased from LC Laboratories. Fludarabine (#14128) was purchased from Cayman Chemical Company. 17-DMAG (A2213) was purchased from ApexBio. 3-(4,5-dimethylthiazol-2-yl)-2,5-diphenyl tetrazolium bromide (MTT) assay was performed to assess cell growth at different time points. Medium in the cell growing wells were replaced by 100 ul of 1X MTT solution in RPMI 1640 without phenol red and incubated at 37°C with 5% $CO_2$ for 3 hr. Then 100 μl solubilization buffer (10% Triton X-100, 0.1N HCl in isopropanol) are applied to each well to dissolve the blue formazan crystals. The absorbance was measured at 570 nm and 650 nm by VARIOSKAN FLASH microplate reader (Thermo Scientific). Bliss Independence (Bliss, 1939) and HSA (Borisy et al., 2003) models were adopted for evaluating interactions between drug pairs, and DiaMOND model (Cokol-Cakmak et al., 2018; Cokol et al., 2017) was used for measuring three-way drug interactions. The excess over Bliss Independence model was calculated as, g12 - (g1 + g2 - g1 x g2 / 100), where g indicates the percentage of growth inhibition, the number indicates the drug component; the excess over HSA model was calculated by subtracting the highest growth inhibition effect of single agent from that of the combination; the DiaMOND model was used for calculating the frictional inhibitory concentration ($FIC_3$), which equals (o1 + o2 + o3)/((e1 + e2 + e3)/3), where o indicates the observed concentration of each component in the combination, and e indicates the expected concentration of individual drugs at certain inhibitory level, which is determined by drug response curves. To generate the drug response curves, the three drugs were combined in a fixed ratio of 1:1:1 of their respective $IC_{50}$ and scaled proportionally. If $FIC_3$ is < 1, the interaction is synergistic; if $FIC_3$ is = 1, the interaction is additive; and if $FIC_3$ is > 1, the interaction is antagonistic.

### Colony formation assay

1,000 OVCAR8-ADR cells were seeded onto one well of a 6-well plate one day prior to drug treatment at indicated doses. Colonies were fixed by ice-cold methanol at −20°C for 30 min and stained by crystal violet. Colony number and area were determined by ImageJ software.

### Drug response study in mice

Six-week-old female BALB/cAnN-nu mice were used in the experiments. $1 \times 10^7$ OVCAR8-ADR cells in 200 μL of PBS mixed with Matrigel (2:1 volume ratio, BD Biosciences, San Jose, CA) were implanted subcutaneously into the right flank of each mouse. 4 weeks after cell inoculation, mice were randomly assigned to 5 subgroups (n = 9 - 12). The administered doses of AZA, FLU and ERL were 0.7 mg/kg, 17 mg/kg, and 8 mg/kg, respectively. The drugs were given once daily by i.p. 5 days per week for 3 weeks. Two-drug and three-drug combination treatments were given at the same schedule. AZA and FLU were suspended in normal saline, while ERL was dissolved in 15% Captisol (Ligand, San Diego, CA). The control mice were treated with the vehicles of the three drugs, following the same schedule. Weights of the excised tumors were measured after euthanasia. Body weight was monitored as a measure of drug toxicity.

### Pseudopupil assay

*gmr-GAL4* female flies were crossed with $w^{1118}$ (control) or *UAS-α-syn* male flies, and raised at 21.5°C on cornmeal medium supplemented with drug(s) or vehicle control. Drug treatment was performed by adding vorinostat (LC Laboratories, V-8477) and/or

17-DMAG (InvivoGen, ant-dgl-25) into 2 mL of the medium at final concentrations of 0.5 μM and 96 μg/ml, respectively. After eclosion, progeny were transferred into a new vial with medium supplemented with fresh drug(s), and the drug(s) were changed every 3-4 days prior to the assay. Eyes of 7- to 11-day-old flies were examined under a light microscope (Olympus CX31) with a 60X oil objective as described previously (Wong et al., 2008). At least 100 ommatidia from 5-10 flies were examined and the number of rhabdomeres were recorded.

### RNA-seq

Total RNAs were isolated from drug-treated OVCAR8-ADR cells by MiniBEST universal RNA extraction kit (Takara). RNA samples were quantified and analyzed using Qubit assay and high-sensitivity DNA chip (Agilent) on an Agilent 2100 Bioanalyzer, respectively. RNA-seq experiments were performed at the Centre for Genomic Sciences (LKS Faculty of Medicine, The University of Hong Kong). The Illumina adaptors of the paired-end raw sequence reads were trimmed by Trimmomatic 0.39. The STAR aligner version 2.7 was used to align the sequence reads to the human genome, where the genome index was built using the primary assembly of Gencode's version 30 release of the human genome. The raw count reads were extracted using the R package Rsubread. R packages EdgeR, limma, and HTSFilter were used for differential expression analysis comparing each of the pairwise and three-way drug combinations with the untreated samples. An FDR < 0.05 filter was applied for the three-way combination versus untreated samples while an FDR < 1 filter was applied for each of the pairwise combinations versus untreated samples. The combinations and the genes were clustered by complete-linkage clustering, where the distance is defined as 1-Pearson correlation. The genes that were at least 20% up- or down- regulated in cells treated with the three-drug regimen when compared to the untreated control were inputted into DAVID web tools for pathway analysis, and the Reactome pathway database was used. The pathway mapping used a p = 0.05 threshold.

### GUIDE-seq

The GUIDE-Seq libraries were constructed using KAPA HyperPlus Kit (Roche) with modifications. Briefly, 400 ng of each DNA samples were fragmented at 37°C for 20 min such that the mode fragment length was approximately 200 - 300 bp. The fragmented DNA samples were then end-repaired and A-tailed to produce 5′-phosphorylated and 3′-dA-tailed by incubating with the End-repair & A-tailing Enzyme at 37°C for 15 min, followed by 65°C for 15 min. Adapters were ligated to the End-repaired and A-tailed DNA fragments using DNA ligase with 20 pmol of annealed adapters at 16°C for 30 min, followed by 22°C for 30 min. Post-ligation cleanup was performed using 1X SPRIselect (Beckman Coulter). The size-selected ligation products were eluted in 20 μL Buffer EB and amplified by two rounds of PCRs for target enrichment.

In PCR1, the ligated DNA fragments were added to 3 μL of 10X PCR buffer, a final concentration of 2 mM of $MgCl_2$, 0.2 mM of dNTP (New England Biolabs), 25 pmol of dsODN enrichment primers (OFF_GSP1+ and OFF_GSP1-) (Choi et al., 2019), 3 Units of Platinum™ Taq DNA Polymerase (Invitrogen) and topped up to a final volume of 30 μL of nuclease free water. The thermo cycling conditions were as follows: initial denaturation at 95°C for 5 min; followed by 14 cycles of 95°C for 30 s and 72 C for 1 min with a touchdown of −1°C per cycle; followed by another 20 cycles of 95°C for 30 s and 58°C for 1 min; and final extension at 72°C for 3 min. The amplified PCR products were washed with 1X SPRIselect and eluted in 30 μL Buffer EB. In PCR2, 15 μL of the SPRI-selected PCR1 products were mixed with 3 μL of 10X PCR buffer, a final concentration of 2 mM of $MgCl_2$, 0.2 mM of dNTP, 25 pmol of dsODN enrichment nested primers (OFF_GSP2+ and OFF_GSP2-), 5 pmol of Y1-48 indexing primer (Table S7), 10 pmol of P7 indexing primer (Choi et al., 2019), 3 Units of Platinum™ Taq DNA Polymerase and topped up to 30 μL with nuclease free water. The thermo cycling parameters were as follows: initial denaturation at 95°C for 5 min; followed by 20 cycles of 95°C for 30 s and 65 C for 1 min; and final extension at 72°C for 3 min. The final library constructs were size selected by 0.7X SPRIselect and eluted in 30 μL of Buffer EB. After quantification by Collbri™ Library Quantification Kit (Invitrogen), the constructed GUIDE-seq libraries were subsequently pooled and sequenced by Illumina NextSeq 500 system. Bioinformatics analyses combining initial custom scripts for sample de-multiplexing, formatting, and identification of off-targets using the GUIDE-seq software were performed as previously described (Choi et al., 2019; Tsai et al., 2015).

## QUANTIFICATION AND STATISTICAL ANALYSIS

Data analyses were performed using GraphPad Prism 7 software (GraphPad Software). Data expressed are mean ± SD, biological replicates (n number) are specified for each experiment in figure legends. Statistical comparisons between two groups were carried out by Student t test, whereas one-way ANOVA followed by Tukey's or Dunnett's post hoc tests were used for comparisons of groups more than two. A P value < 0.05 was considered as statistically significant.